Journal of Medicinal Chemistry

Drug Annotation

Discovery and characterization of AZD6738, a potent inhibitor of ataxia telangiectasia mutated and rad3 related (ATR) kinase with application as an anti-cancer agent

Kevin Michael Foote, J. Willem M. Nissink, Thomas M. McGuire, Paul Turner, Sylvie Guichard, James T. Yates, Alan Lau, Kevin Blades, Dan Heathcote, Rajesh Odedra, Gary Wilkinson, Zena Wilson, Christine Wood, and Philip J Jewsbury

J. Med. Chem., **Just Accepted Manuscript** • DOI: 10.1021/acs.jmedchem.8b01187 • Publication Date (Web): 22 Oct 2018

Just Accepted

ACS Publications

is published by the American Chemical Society. 1155 Sixteenth Street N.W., Washington, DC 20036

Discovery and characterization of AZD6738, a potent inhibitor of ataxia telangiectasia mutated and rad3 related (ATR) kinase with application as an anti-cancer agent

Kevin M. Foote[a#], J. Willem M. Nissink[a], Thomas McGuire[a], Paul Turner[a], Sylvie Guichard[b£], James W. T. Yates[c], Alan Lau[b], Kevin Blades[a$], Dan Heathcote[d], Rajesh Odedra[d^], Gary Wilkinson[a&], Zena Wilson[b], Christine M. Wood[a], and Philip J Jewsbury[a]*

[a] Chemistry, Oncology, IMED Biotech Unit, AstraZeneca, Cambridge Science Park, 310 Milton Rd, Milton, Cambridge, CB4 0WG, UK

[b] Bioscience, Oncology, IMED Biotech Unit, AstraZeneca, Chesterford Research Park, Little Chesterford, Cambridge, CB10 1XL, UK

[c] DMPK, Oncology, IMED Biotech Unit, AstraZeneca, Chesterford Research Park, Little Chesterford, Cambridge, CB10 1XL, UK

[d] Discovery Sciences, IMED Biotech Unit, AstraZeneca, Cambridge Science Park, 310 Milton Rd, Milton, Cambridge CB4 0WG , UK

Current affiliation: Pharmaron, Drug Discovery Services Europe, Hertford Road, Hoddesdon, Hertfordshire, EN11 9BU , UK

£ Current affiliation: Forma Therapeutics, 500 Arsenal Street, Watertown, MA 02472, Boston, USA

$ Current affiliation: AMR Centre Ltd, 19B70, Mereside Alderley Park, Alderley Edge, SK10 4T, UK

& Current affiliation: Bayer, Müllerstraße 178, 13353, Berlin, Germany

^ Current affiliation: Evotec, 114 Innovation Drive, Milton Park, Abingdon Oxfordshire OX14 4RZ, UK

ABSTRACT

The kinase ataxia telangiectasia mutated and rad3 related (ATR) is a key regulator of the DNA-damage response and the apical kinase which orchestrates the cellular processes that repair stalled replication forks (replication stress) and associated DNA double-strand breaks. Inhibition of repair pathways mediated by ATR in a context where alternative pathways are less active is expected to aid clinical response by increasing replication stress. Here we describe the development of the clinical candidate **2** (AZD6738), a potent and selective sulfoximine morpholino-pyrimidine ATR inhibitor with excellent preclinical physicochemical and pharmacokinetic (PK) characteristics. Compound **2** was developed improving aqueous

solubility and eliminating CYP3A4 time-dependent inhibition starting from the earlier described inhibitor **1** (AZ20). The clinical candidate **2** has favorable human PK suitable for once or twice daily dosing and achieves biologically effective exposure at moderate doses. Compound **2** is currently being tested in multiple Phase I/II trials as an anti-cancer agent.

INTRODUCTION

Human cells are constantly exposed to DNA-damage events as a result of environmental and endogenous factors. In order to suppress genomic instability, an integrated group of biological pathways collectively called the DNA-damage response (DDR), has evolved to recognize, signal, and promote the repair of damaged DNA.[1, 2] DNA-damage leads to cell death if sufficiently high and left unrepaired and is the concept behind DDR inhibition for cancer therapy. Tumor cells are sensitized to DDR based therapies through a combination of relatively rapid proliferation and DDR pathways that may already be functionally compromised. Ataxia telangiectasia and Rad3-related (ATR) is a serine/threonine-protein kinase belonging to the phosphatidylinositol 3-kinase-related kinase (PIKK) family of proteins and is a key regulator of DNA replication stress response (RSR) and DNA-damage activated checkpoints.[3, 4] Replication stress, a hallmark of cancer,[5] may occur in tumors through oncogene drivers or induced exogenously through treatment with DNA-damaging drugs or ionizing radiation (IR). Persistent replication stress leads to DNA breaks which if left unresolved are highly toxic to cells. In recent years potent and selective inhibitors of ATR (Scheme 1) have been developed

from orthogonal chemical series demonstrating preclinical *in vivo* proof of concept. These pivotal compounds and studies have been extensively reviewed,[6-9] and reveal synthetic lethality of ATR inhibitors on tumors with p53-mutations or Ataxia telangiectasia mutated (ATM) loss-of-function,[10, 11] as well as synergy in combination with a broad range of replication stress inducing chemotherapy agents such as platinums,[12] ionizing radiation,[13, 14] and with novel agents such as the PARP inhibitor olaparib.[15]

Scheme 1. ATR inhibitors; **2**, **3** and **4** are undergoing clinical testing

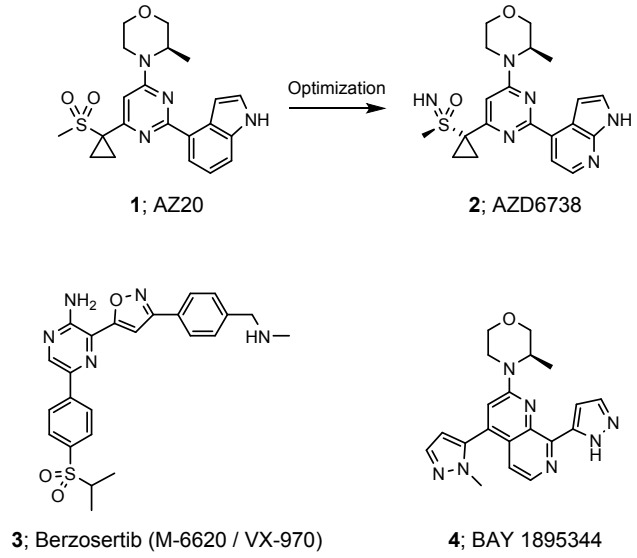

We have previously described a series of potent and selective ATR inhibitors, exemplified by **1** (AZ20), from the sulfonylmethyl morpholino-pyrimidine series.[16] Compound **1**, and close analogues,[17] were shown to inhibit the growth of ATM-deficient xenograft models at well tolerated doses. However, we did not consider compound **1** of sufficient quality for further

development due to low aqueous solubility and high-risk for drug-drug interactions (DDI) resulting from Cytochrome P450 3A4 (CYP3A4) time-dependent inhibition (TDI). In this report we describe our further studies to identify ATR inhibitors with the requisite properties suitable for clinical development that led to the discovery of **2** (AZD6738). The sulfoximine morpholino-pyrimidine **2**, along with the aminopyrazine **3** (berzosertib, M-6620 / VX-970), originating from Vertex and licensed to Merck KGaA, and most recently the naphthyridine **4** (BAY 1895344) from Bayer,[18] have entered human studies. These compounds are being explored in early-phase clinical trials as single-agents and in combination with standard of care (SOC) and novel agents.[8, 9]

RESULTS

Compounds **1**, **5**, **6**, **8**, **9** and **10** (Table 1) and intermediates **39**, **46** – **49**, **70** were prepared as described previously.[16] Compounds **7**, **17** and **18** were prepared as shown in Scheme 2 and compounds **11** – **16** were prepared as shown in Scheme 3. Intermediates **43** – **45** were prepared starting from the dichloropyrimidine **39**. Suzuki coupling with 2-cyclohexenyl-4,4,5,5-tetramethyl-1,3,2-dioxaborolane led to **40** while S_NAr reaction with 8-oxa-3-azabicyclo[3.2.1]octane and 3-oxa-8-azabicyclo[3.2.1]octane afforded **41** and **42** respectively with no evidence of substitution at the 2-position. Cyclopropanation with 1,2-dibromoethane and strong base afforded **43** – **45**. The 2-arylpyrimidine test compounds were synthesized by Suzuki coupling between the 2-chloropyrimidine substrates **43** – **48** and the corresponding

boronic acid or esters which were either purchased or prepared from the corresponding aryl bromides using literature methods.[19]

1-*H*-benzimidazole test compounds **19** – **30** (Table 4) were made as shown in Scheme 4 and 5. Cyclopropanation of **49** led to **50** where reaction with 3(*R*)-methyl morpholine followed by sodium tungstate catalysed oxidation of the sulfide proceeded well to afford **51** without over-oxidation of the pyrimidine ring. Reaction with 1*H*-benzo[*d*]imidazol-2-amine or *N*-methyl-1*H*-benzo[*d*]imidazol-2-amine led directly to compounds **19** and **21** respectively; compound **19** was derivatized to the *N*-acetyl **20**. Benzimidazoles **22** – **30** were made starting from the 2-chloropyrimidine intermediate **47** (Scheme 5). Buchwald-Hartwig coupling with the appropriate substituted 2-nitroaniline utilising the xantphos ligand system afforded intermediates **52** – **60**. Reduction of nitro to amino was achieved under indium catalyzed transfer hydrogenation conditions or with zinc in acetic acid to give the corresponding anilines **61** – **69** which were then cyclized using cyanogen bromide to afford compounds **22** – **30**.

The iodobenzyl compound **70** was used as the starting point for the synthesis of sulfoxides **31**, **32** and sulfoximines **2**, **33** – **36** (Scheme 6). Displacement of the iodide in **70** with sodiumthiomethoxide gave sulfide **71** in high yield which was then oxidized to the corresponding sulfoxide **R/S-72** with sodium metaperiodate. Compounds were either made as a mixture of diastereoisomers and separated by chiral chromatography or prepared starting with the appropriate chirally pure sulfoxide. The mixture of sulfoxide diastereoisomers **R/S-72** were readily separable by chiral chromatography or vapor diffusion crystallization to afford **R-72** as a white crystalline solid and **S-72** as an oil. The stereochemistry of **R-72** was confirmed

by X-ray structure (Supplementary Figure S2). Later, a biocatalytic process to the chiral sulfoxide **R-72** was developed from **71** on large scale.[20] Cyclopropanation led to **R/S-73** followed by Suzuki coupling to afford the test compounds **31** and **32**. The sulfoximine moiety was introduced starting from the sulfoxides via rhodium catalyzed nitrene insertion.[21] This proceeded with complete retention of stereochemistry and worked equally well either starting from the mixture of sulfoxide diastereoisomers to afford **R/S-74** or from single diastereoisomer **R-72** to afford **R-74**. Cyclopropanation resulted in rapid removal of the trifluoroamide group, to give **R/S-75** followed by Suzuki reaction led to test compounds **2**, **33** and **34** or reaction with *N*-methyl-benzo[*d*]imidazole-2-amine led to **35** and **36**.

Scheme 2[a]

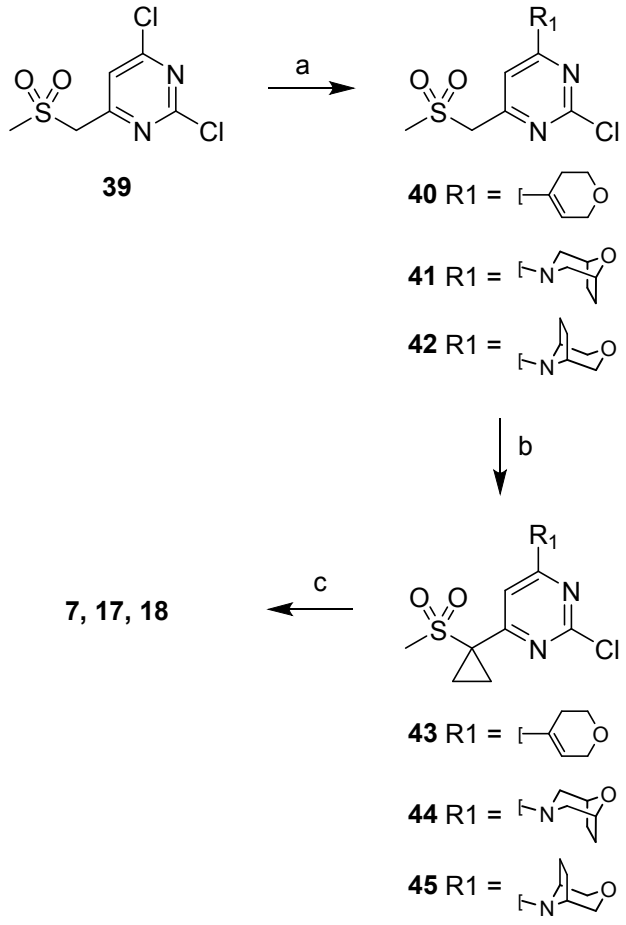

[a] Reagents: (a) compound **40**: $(Ph_3P)_4Pd$, 2-(3,6-dihydro-2*H*-pyran-4-yl)-4,4,5,5-tetramethyl-1,3,2-dioxaborolane, Cs_2CO_3, 1,4-dioxane, water, rt; compounds **41** and **42**: 8-oxa-3-azabicyclo[3.2.1]octane or 3-oxa-8-azabicyclo[3.2.1]octane respectively, Et_3N, DCM, rt; (b) compound **43**: 1,2-dibromoethane, NaH, DMF, 0 °C → rt; compounds **44** and **45**: 1,2-dibromoethane, 50% NaOH (aq.), tetraoctylammonium bromide, DCM, rt; (c) compound **7**: $(Ph_3P)_2PdCl_2$, 1*H*-indol-4-yl boronic acid, Na_2CO_3 (aq.), 4:1 DME:water, microwave, 110 °C; compounds **17** and **18**: $(Ph_3P)_4Pd$, 4-(4,4,5,5-tetramethyl-1,3,2-dioxaborolan-2-yl)-1*H*-pyrrolo[2,3-*c*]pyridine, Na_2CO_3 (aq.), 1,4-dioxane, 95 °C.

Scheme 3[a]

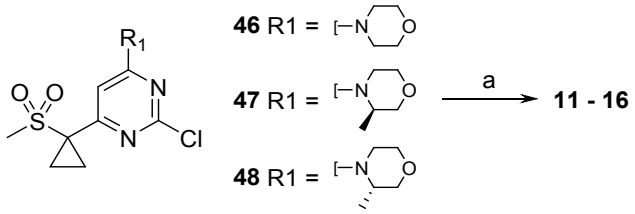

[a] Reagents: (a) compound **11**: $(Ph_3P)_4Pd$, 1*H*-pyrrolo[2,3-*b*]pyridine-4-ylboronic acid, Na_2CO_3 (aq.), 1,4-dioxane, 90 °C; compound **12**: 1*H*-benzo[*d*]imidazol-2-amine, Na_2CO_3, DMA, 160 °C, microwave; compound **13**: $(Ph_3P)_2PdCl_2$, 1*H*-pyrrolo[2,3-*b*]pyridine-4-ylboronic acid, Na_2CO_3 (aq.), 4:1 DME:water, 110 °C, microwave; compound **14**: 2-dicyclohexylphosphino-2',4',6'-triisopropylbiphenyl, bis(dibenzylideneacetone)palladium(0), 4-bromo-1*H*-pyrrolo[2,3-*c*]pyridine, KOAc, bis(pinacolato)diboron, dioxane, 100°C followed by compound **46**, $(Ph_3P)_4Pd$, Na_2CO_3 (aq.), 100 °C; compound **15**: 1,1'-bis(diphenylphosphino)ferrocenedichloropalladium, 4-bromo-1*H*-pyrrolo[2,3-*c*]pyridine, KOAc, bis(pinacolato)diboron, dioxane, 95 °C followed by compound **47**, $(Ph_3P)_4Pd$, Na_2CO_3 (aq.), 95 °C; compound **16**: $(Ph_3P)_4Pd$, Na_2CO_3 (aq.), 4-(4,4,5,5-tetramethyl-1,3,2-dioxaborolan-2-yl)-1*H*-pyrrolo[*2,3-c*]pyridine, dioxane, 95 °C.

Scheme 4[a]

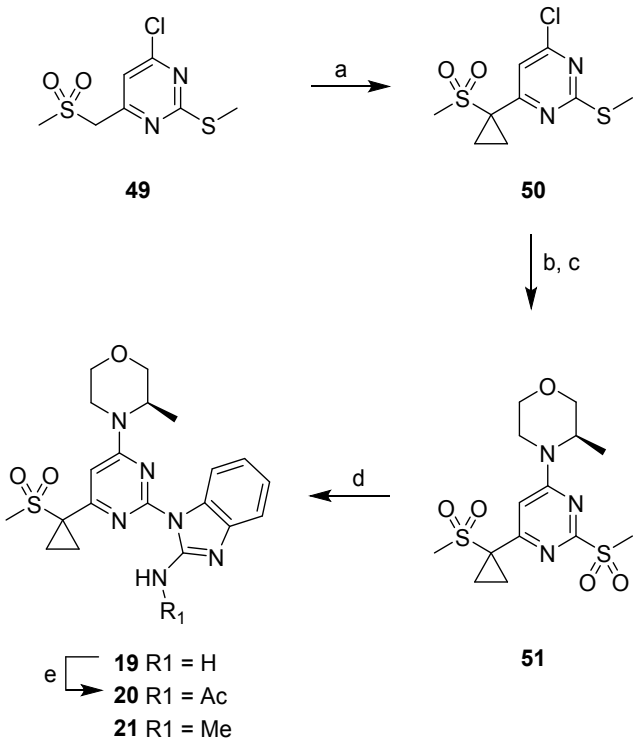

[a] Reagents: (a) 1,2-dibromoethane, 50% NaOH (aq), tetraoctylammonium bromide, toluene, 60 °C; (b) (*R*)-3-methylmorpholine, DIPEA, 1,4-dioxane, 80 °C; (c) $NaO_4W{\cdot}2H_2O$, Bu_4NHSO_4, EtOAc, H_2O_2, 0 °C → rt; (d) compound **19**: 1*H*-benzo[*d*]imidazol-2-amine, Cs_2CO_3, DMA, 110 °C, microwave; compound **21**: N-methyl-1*H*-benzo[*d*]imidazol-2-amine, Cs_2CO_3, DMA, 90 °C; (e) DMAP, Ac_2O, 90 °C.

Scheme 5[a]

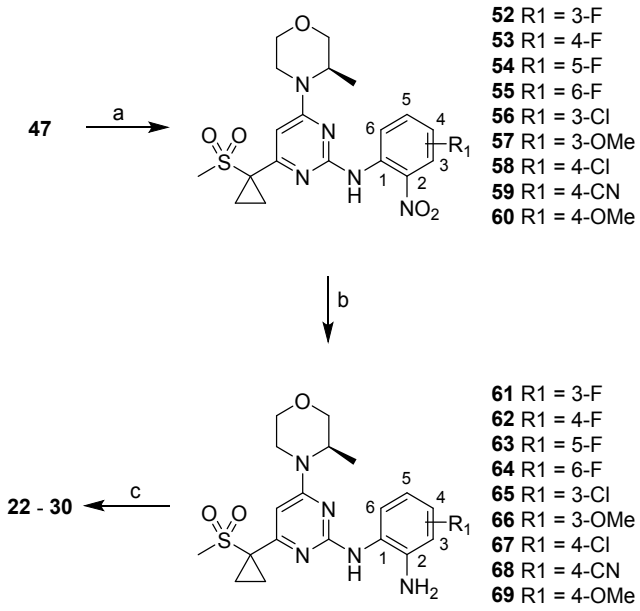

[a] Reagents: (a) Substituted 2-nitroaniline, $Pd(OAc)_2$, xantphos, Cs_2CO_3, 1,4-dioxane, 80 °C, microwave; (b) Zn, AcOH, rt or In, NH_4Cl (aq.), EtOH, reflux; (c) Cyanogen bromide, MeOH, rt.

Scheme 6[a]

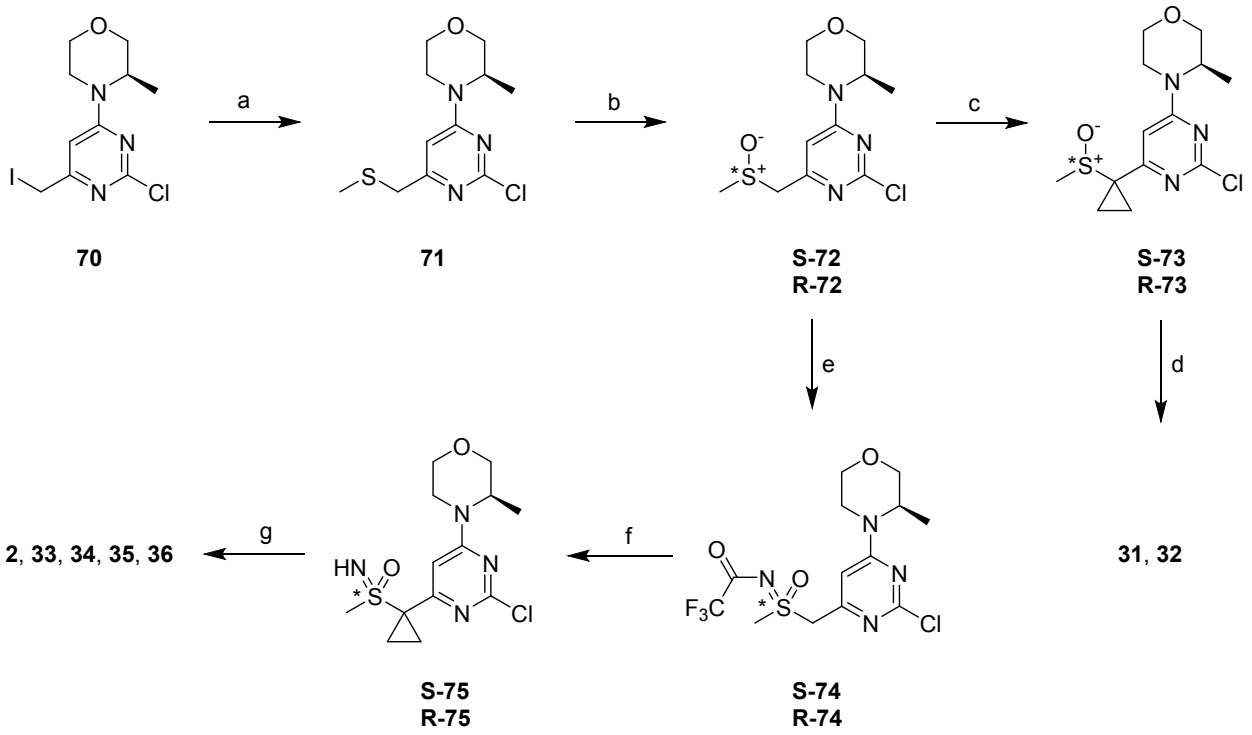

[a] Reagents: (a) NaSMe, DMF, rt; (b) $NaIO_4$, EtOAc, MeOH, H_2O, rt; (c) 1,2-dibromoethane, 50% NaOH (aq.), tetraoctylammonium bromide, 2-Me-THF, 60 °C; (d) X-Phos 2nd gen. precatalyst, 4-(4,4,5,5-tetramethyl-1,3,2-dioxaborolan-2-yl)-1*H*-pyrrolo[2,3-*b*]pyridine, Cs_2CO_3, 1,4-dioxane:H_2O (4:1), 90 °C; (e) trifluoroacetamide, iodobenzene diacetate, $Rh(OAc)_2$ dimer, MgO, *iso*-propylacetate, 80 °C; then 7M NH_3 in MeOH, rt; (f) NaOH (50% aq.), 1,2-dibromoethane, tetra-octylammonium bromide, mTHF, rt; (g) compound **33**: $(Ph_3P)_2PdCl_2$, 2M Na_2CO_3, 4-(4,4,5,5-tetramethyl-1,3,2-dioxaborolan-2-yl)-1-tosyl-1*H*-pyrrolo[2,3-*b*]pyridine, DME:H_2O (4:1), 90 °C then 2M NaOH (aq.), 50 °C; compound **34**: 1*H*-pyrrolo[2,3-*b*]pyridin-4-ylboronic acid, $(Ph_3P)_2PdCl_2$, 2M Na_2CO_3, DME:H_2O (4:1), 90 °C; compound **35** and **36**: Cs_2CO_3, N-methyl-1*H*-benzo[*d*]imidazol-2-amine, DMA, 80 °C.

DISCUSSION

Compound **1** is a potent ATR inhibitor with excellent kinase selectivity and free exposure and is a useful tool compound to explore ATR pharmacology *in vivo*.[16] However, compound **1** was also found to be a time-dependent inhibitor of CYP3A4 and to suffer from low aqueous

solubility. Inhibition of CYP3A4, particularly mechanism based inhibition, is a concern for clinical DDI,[22-24] whereas low solubility limits the maximum absorbable dose (D_{abs}).[25] These properties increase risk of failure in clinical development and compound **1** was therefore not considered a suitable candidate for clinical-enabling studies. Eliminating CYP3A4 TDI and achieving high aqueous solubility at the same time maintaining high ATR potency, excellent specificity and the attractive pharmacokinetic properties exhibited by **1**, were the key medicinal-chemistry design goals in the optimization phase.

CYP TDI has been observed as a common feature in kinase inhibitors with CYP3A4 being the most commonly inhibited isoform.[26] CYP TDI is associated with the formation of covalent (or reversible-covalent) adducts to heme or protein following metabolic activation.[23, 24] In addition to the risk of DDIs, formation of reactive metabolites is a causative factor for idiosyncratic drug toxicity.[23, 27] The risk and impact of clinical DDI will be determined by overall drug disposition, dose, regimen and target patient population. While compound **1** clearly demonstrated TDI of CYP3A4 when incubated at 10 μM in human microsomes,[16] we did not fully characterize this activity or model in detail the human PK and predicted clinical dose to understand the magnitude of the expected clinical DDI. We anticipated ATR inhibitors would be combined with cytotoxic and targeted drugs in the clinic. As DDI arising from inhibition of CYP3A4 would complicate co-dosing of such agents and many likely co-medicants,[28] we set out to remove this undesirable activity.

The indole and morpholine groups were thought particularly vulnerable to metabolic activation. The susceptibility of cyclic tertiary amines such as morpholine to α-carbon

oxidation, generating reactive iminium ion intermediates is well described.[29-31] Indoles are known to undergo ring hydroxylation particularly at C-5 and/or C-6 positions;[32] these species could arise via reactive epoxides and could also lead to quinone-like reactive intermediates following additional bioactivation. Oxidation of indole has also been observed at C-2 or C-3, presumably via the corresponding epoxide, and further oxidation and/or oxidative ring cleavage can lead to anthranilic acid products. The putative metabolic vulnerability of morpholine and indole presented us with a potentially insoluble problem as our previous work clearly demonstrated the importance of both groups to ATR potency.[16]

Reactive metabolites formed from bioactivation are generally electrophilic in character and highly unstable. Trapping experiments can be used to detect and characterize metabolites whereby a compound is incubated in human liver microsomal preparations and any reactive metabolites generated are trapped by specific added nucleophiles. Orthogonal nucleophiles are used to trap the different electrophilic species arising from bioactivation of chemical substrates. The nucleophiles commonly used are glutathione (GSH), a soft nucleophile efficient at trapping soft electrophiles such as epoxides, cyanide to trap iminium species arising from oxidation of tertiary amines and methoxyamine to effectively trap aldehyde products as Schiff bases.[33] These screens provide valuable mechanistic information to support rational medicinal chemistry design. When **1** was incubated with human liver microsomes, adducts with GSH but not cyanide were detected. Whilst the mechanisms of bioactivation and TDI may not necessarily overlay, the formation of GSH adducts implicates the indole group, likely through ring oxidation.

We had systematically explored the structure activity relationships (SAR) in the morpholino-pyrimidine pharmacophore, varying each of the substituents on the pyrimidine core. These compounds now allowed facile investigation into the molecular features in **1** responsible for CYP3A4 TDI, independent of ATR potency.

Table 1. Morpholine and C-2 heterocycle CYP3A4 TDI SAR

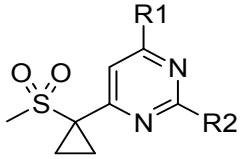

Compound	R1	R2	ATR IC_{50} (μM)[a]	ATR cell IC_{50} (μM)[b]	$LogD_{7.4}$[c]	CYP3A4 % TDI, 10 μM[d]
1	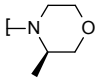	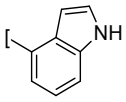	0.005	0.061*	2.5#	50
5	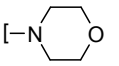	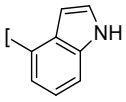	0.008	0.29	2.3	38
6	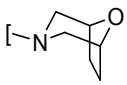	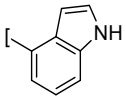	0.007	0.11	2.6	53
7	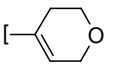	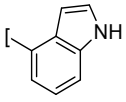	0.018	0.27	2.9	49
8	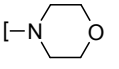	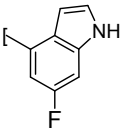	0.015	0.13	ND	61
9	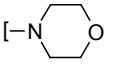	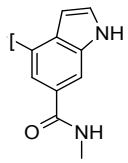	0.14	16.5	1.6	<9
10	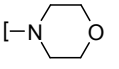	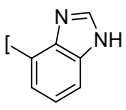	0.18	6.2	2.2	<11

11	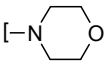	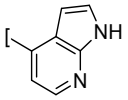	0.037	0.35	2.2	<11
12	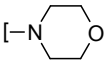	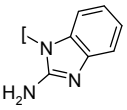	0.003	0.051	2.2	17[†]

[a]Uncertainty (95% confidence) for pIC_{50} measurements is 0.38 (2.4-fold) based on an average of two repeat occasions per compound. [b] Uncertainty (95% confidence) for pIC_{50} measurements is 0.7 (4.6-fold) based on at least two repeat measurements per compound (median number of repeats across tables is 3). The data presented is from a variation of the ATR cell assay described in Ref. [16](see experimental section). A good correlation is observed between ATR cell assay versions; N=41 compounds from morpholino-pyrimidine series, correlation: 0.94, mean difference: -0.084 pIC50. [*]Compound **1** IC_{50} = 0.050 μM in the earlier version reported.[16] [c] $LogD_{7.4}$ assay: lipophilicity was determined using the 'shake-flask' method. Plated aliquots of sample are dried down and octanol and water are added. Sample content of the phases is determined by LC/MS/MS after stirring, equilibration, and separation of phases by centrifuge. Full description of the assay can be found in the Supplementary Materials. An excellent correlation is observed between versions of the $LogD_{7.4}$ methods; N=23

compounds from the morpholino-pyrimidine series, correlation: 0.96, mean difference: -0.075. #Compound **1** $LogD_{7.4}$ = 2.7 using the earlier methodology (Ref. [16]). ND = not determined. [d] Mean value (N≥2) unless otherwise stated. Compounds were pre-incubated at 10 μM with human liver microsomes (1 mg/mL) with and without NADPH (5 mM) for 30 min at 37 °C followed by 15 min incubation with 10 μM midazolam; analysis of 1-hydroxymidazolam was performed using liquid chromatography-tandem mass spectrometry.[34] No activity detected vs. control for 1A2, 2C19, 2C9, and 2D6. † Result for compound **12** was just above background level in test 1 and below background level (<11%) in test 2; result for test 1 shown.

The unsubstituted and 3(*R*)-methyl substituted morpholines (compounds **5** and **1** respectively) both show clear CYP3A4 TDI activity when incubated at 10 μM in human liver microsomes using a standard liquid chromatography-tandem mass spectrometric endpoint (Table 1).[34] Introducing structural architecture to eliminate reactive moieties resulting from oxidation on the morpholine ring, for example by modification of the methylene adjacent to the oxygen atom using the bridged morpholine **6** or removal of the nitrogen heteroatom by substitution of morpholine for the 3,6-dihydro-2*H*-pyran **7**, did not eliminate CYP3A4 TDI activity compared with morpholine. The dihydropyran and bridged morpholines, both of which have been described as morpholine isosteres in mTOR inhibitor series,[35, 36] are equivalent in ATR potency to unsubstituted morpholine but at the price of higher lipophilicity. The impact of blocking and/or deactivating substituents on the indole ring was investigated. Simple ring substituents that retain ATR potency, for example the 6-fluoro indole **8**, did not reduce CYP3A4 TDI. In contrast, addition of a polar and deactivating group such as acetamido **9** and replacement of the indole, for example with benzimidazole **10**, which has equivalent lipophilicity to the indole **5**, led to undetectable CYP3A4 TDI activity. In both cases

ATR potency was also significantly reduced but these results supported the notion that the indole ring was the likely key contributor to CYP3A4 TDI. We discovered the 7-azaindole (1*H*-pyrrolo[2,3-*b*]pyridine) **11** retains the ATR potency of the indole while effectively eliminating CYP3A4 TDI. In addition, through a wider campaign to identify ATR-active indole isosteres, the 2-amino-*N*1-substituted benzimidazole **12** was found to have no or weak detectable 3A4 TDI. This variant was also found to possess superior cellular potency without increasing lipophilicity compared with the indole **5**. Unknown to us at the time, Safina *et al.*[37] had developed a series of PI3Kδ-specific morpholinopyrimidines substituted with 4-indole that were also found to be potent CYP3A4 TDIs and further determined that the 4-indole group was associated with this activity. In contrast to our own findings, replacement of the indole with 7-azaindole in the PI3Kδ series did not attenuate CYP3A4 TDI. The apparent conflicting results are a reminder that metabolic activation is complex, and SAR may not be simplified to contributions of individual functional groups. It is whole-molecule structure and properties that determine metabolic fate. However, in our efforts towards identifying an ATR inhibitor candidate for human studies, both the 7-azaindole **11** and 2-aminobenzimidazole **12** became productive leads for optimization.

In the 7-azaindole series, the SAR was found to mirror that determined for indole with cellular potency increasing for the corresponding 3-(*R*) methyl morpholine **13** (Table 2). Pleasingly we could not detect CYP3A4 TDI activity for this compound. Measured lipophilicity for **13** is unchanged in comparison to **1** and unsurprisingly solubility remains low.

Table 2. Azaindole SAR

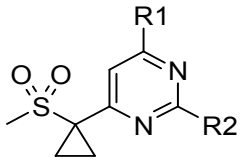

Compound	R1	R2	ATR IC_{50} (μM)[a]	ATR cell IC_{50} (μM)[b]	$LogD_{7.4}$	LLE[c]	Solubility pH7.4 (μM)[d]	CYP3A4 % TDI, 10 μM
1	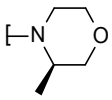	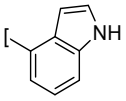	0.005	0.061	2.5	4.7	10	50
13	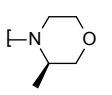	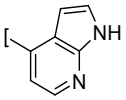	0.005	0.10	2.6	4.4	8	<10
14	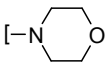	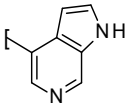	0.005	0.085	1.8	5.3	130	<15
15	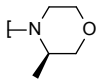	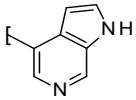	0.002	0.012	2.1	5.8	108	<20
16	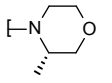	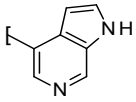	ND	0.36	2.2	4.2	165	ND
17	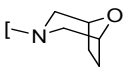	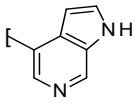	ND	0.086	2.2	4.9	>1510	ND
18	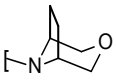	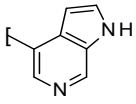	ND	0.26	2.1	4.5	98	ND

[a,b] For assay uncertainty, see footnotes in Table 1 [c] Lipophilicity ligand efficiency (LLE): ATR cell pIC_{50} – $LogD_{7.4}$. [d] Solid material was agitated in 0.1 M pH 7.4 phosphate buffer for 24 h, double centrifuged, and the supernatant analyzed for compound concentration by LC–UV–MS. Crystallinity assessed by polarized light microscopy of remaining solid. Full description is provided in Supplementary Materials. Lowest solubility given in the table where multiple measurements were taken: N≥3 for compounds **1**, **13**, **15**; N=1 for compounds **14**, **16**, **17**, **18**. ND: not determined.

Substitution with the 6-azaindole (1*H*-pyrrolo[2,3-*c*]pyridine) isomer surprisingly resulted in compounds with much improved cellular potency compared with the corresponding indole and 7-azaindole. Moreover the 6-azaindole series combines improved potency with reduced lipophilicity and improved aqueous solubility (compounds **14** – **18**, Table 2; note: the very high solubility result for compound **17** is most likely an outlier that we speculate is due to low crystallinity) while also having no detectable CYP3A4 TDI. It is interesting to observe a seemingly small structural change delivering such a significant effect on both potency and physicochemical properties.[38] Directionality of the hydrogen bond acceptor nitrogen in the azaindole isomers is changed relative to the morpholine hinge binder offering the potential to impact key interactions to the protein. Recent structures of ATR-mimicking PI3K mutants,[39] and an ATR cryo-EM,[40] structure suggest that the difference in potency between the azaindoles isomers can be explained by their interaction with Asp2335, potentially mediated by a water molecule. 6-Azaindole is also considerably more basic than 7-azaindole (pKa 7.9 and 4.6 respectively[41]) resulting in an expected change in ionization state at physiological pH and concomitant effects on $LogD_{7.4}$ and solubility. The unsubstituted morpholine 7-azaindole **14** demonstrated excellent ATR cellular potency (IC_{50} <100 nM) and again the established morpholine SAR translated, with a significant increase in potency observed when 3-(*R*) methyl morpholine was employed over the 3-(*S*) methyl isomer (compounds **15** and **16** respectively). The bridged morpholines, compounds **17** and **18**, retained potency compared to morpholine **14** and the reduced lipophilicity provided by the 6-azaindole group led to compounds with a good overall balance of properties. It is noticeable from the compounds

shown in Table 2 that the hitherto excellent ATR enzyme to cell correlation breaks down. We had high confidence in the cellular assay measuring inhibition of CHK1 phosphorylation, a direct substrate of ATR, in response to a DNA-damage stimulus. Presumably, with the more potent compounds, the IC_{50} is below the detection threshold (tight binding limit) of the enzyme assay. Therefore, at this stage of the optimization phase the cellular assay was primarily used to drive chemistry in conjunction with lipophilicity and physicochemical driven properties of aqueous solubility, permeability and metabolic stability. The 3-(*R*)-methyl morpholine 6-azaindole **15** stood out in combining excellent cellular potency and moderate lipophilicity (LLE = 5.8) with improved aqueous solubility and no measureable CYP3A4 TDI and represented a significant advancement over the indole lead **1**.

The benzimidazole head group utilized in compound **12**, substituted at the 2-position with amino or alkyl substituents on a morpholino-pyrimidine core was described in a series of anti-tumor agents with PI3K activity from Zenyaku Kogyo.[42] We discovered the novel methylsulfonylmethyl morpholino-pyrimidine **12** to possess excellent ATR potency (Table 1) albeit with some class 1 PI3K inhibitory activity (e.g. PI3Kα IC_{50} = 0.24 μM). Substitution on the morpholine hinge binder has been shown to affect PI3K activity,[16, 36] thus the 3(*R*)-methyl morpholine 2-aminobenzimidazole (compound **19**, Table 3) became a key compound to make that was subsequently shown to possess greatly improved ATR potency and selectivity over PI3Kα (ATR cell IC_{50} = 0.015 μM, PI3Kα IC_{50} = 9 μM).

Table 3. Benzimidazole C2 SAR

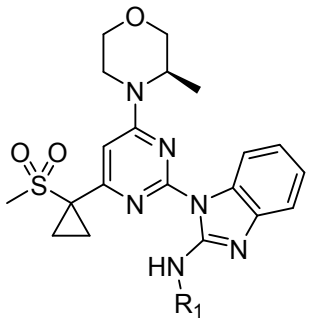

Compound	R1	ATR IC_{50} (μM)[a]	ATR cell IC_{50} (μM)[b]	$LogD_{7.4}$	LLE	Solubility pH7.4 (μM)[c]	CYP3A4 % TDI, 10 μM
19	H	0.001	0.015	2.5	5.3	20	20[†]
20	Ac	0.014	0.017	1.8	6.0	7	<17
21	Me	0.002	0.008	2.8	5.3	49	<18

[a,b] For assay uncertainty, see footnotes in Table 1 [c] Lowest solubility result is given in the table where multiple measurements were taken: N=2 for compound **21**; N=1 for compounds **19**, **20**. [†] Result for compound **19** was just above background level in test 1 and below background level (<17%) in test 2; result shown for test 1.

The potency improvement relative to indole is achieved without increasing lipophilicity; compound **19** shows borderline CYP3A4 TDI and aqueous solubility is not significantly improved compared to indole **1**. Substitution on the amino group with acetyl (compound **20**) or methyl (compound **21**) were well tolerated with no loss of cellular potency and in the case of the *N*-acetyl **20**, led to higher LLE. Moreover, we did not detect CYP3A4 TDI for either of the substituted 2-amino-benzimidazole compounds. While a relatively modest improvement in aqueous solubility was perhaps evident, particularly for *N*-methyl **21**, aqueous solubility was not robustly improved compared with indole.

Substitution on the benzimidazole aryl ring was explored for effects on potency and to address a theoretical concern that the naked aryl ring might be susceptible to metabolic

instability. The result of systematic substitution on the aryl ring of the benzimidazole group with fluorine is shown in Table 4.

Table 4. Benzimidazole ring SAR

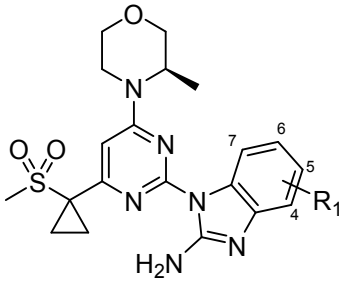

Compound	R1	ATR IC_{50} (μM)[a]	ATR cell IC_{50} (μM)[b]
19	H	0.001	0.015
22	4-F	0.010	0.13
23	5-F	0.002	0.035
24	6-F	0.008	0.12
25	7-F	0.090	5.1
26	4-Cl	0.017	5.3
27	4-OMe	0.27	5.3
28	5-Cl	0.021	0.87
29	5-CN	4.0	>30
30	5-OMe	0.55	15

[a,b] See footnotes a,b in Table 1 for assay uncertainty; repeat measurements: N=2 for compound **19**; N=1 for compounds **22** – **30**.

A 5-F substituent (compound **23**) retains the same level of ATR potency compared with unsubstituted benzimidazole **19**. While 4-F and 6-F (compounds **22** and **24** respectively) retain a degree of ATR potency the 7-F analogue (compound **25**) is significantly less potent. A broader range of substituents in positions 4- and 5- (exemplified by compounds **26** – **30**, Table 4) were

then made to probe into the protein further but for all these examples reduced ATR potency was seen.

In the solid state, methylsulfone compounds such as **1** display a centrosymmetric methylsulfone to methylsulfone contact (in addition to ring-ring stacking and a hydrogen bonding network between indole N-H and sulfone oxygen) associated with high melting points and low solubility.[16] Our SAR study of the indole series demonstrated that specific changes around the methyl sulfonyl moiety (e.g. addition of charged substituents) could improve physicochemical properties, but these changes ultimately led to reduced potency and/or attenuation of other fundamental properties such as permeability leading to low oral exposure. However, we had yet to attempt specific changes to the sulfone group, for example replacement with sulfoxide or sulfoximine whereby one of the oxygen atoms is replaced with nitrogen. We hypothesized that such changes could disrupt the observed solid-state contacts albeit at the complication of introducing additional chirality and with uncertain impact on target potency.

Table 5. Sulfoxide and sulfoximine SAR

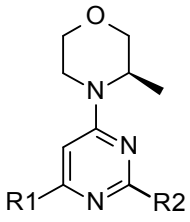

Compound	R1	R2	ATR	ATR cell	$LogD_{7.4}$	LLE	Solubility	CYP3A4 %

			IC_{50} (μM)[a]	IC_{50} (μM)[b]			pH7.4 (μM)[c]	TDI, 10 μM
13	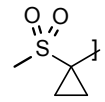	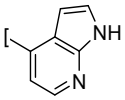	0.005	0.10	2.6	4.4	8	<10
31	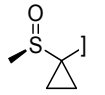	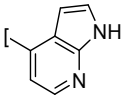	0.016	0.18	2.5	4.2	240	ND
32	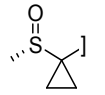	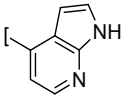	0.011	0.090	2.5	4.6	198	ND
2	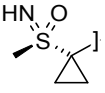	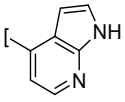	0.004	0.074	1.9	5.2	661	<20
33	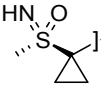	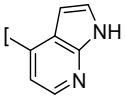	ND	0.24	1.8	4.8	179	<11
34	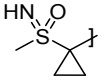	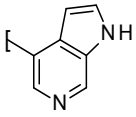	ND	0.014	1.4	6.5	>2120	ND
35	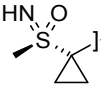	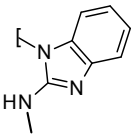	0.006	0.009	2.1	6.0	>780	<20
36	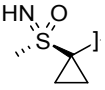	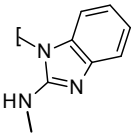	ND	0.023	2.1	5.5	933	ND

[a,b] See footnotes in Table 1 for assay uncertainty. ND = not determined. [c] Lowest solubility result is given in the table where multiple measurements were taken: N≥2 for compound **13**, **2**, **33**, **35**; N=1 for compounds **31**, **32**, **34**, **36**.

The diastereomeric sulfoxides in the 7-azaindole series, compounds **31** and **32** (Table 5), were found to retain ATR potency compared with the corresponding sulfone **13** with no change in measured lipophilicity. These sulfoxides were also found to have high aqueous solubility though it proved challenging to generate stable crystalline forms and therefore the apparent

improvement compared with the corresponding sulfones was treated with caution. The sulfoxides are highly permeable and have high exposure from oral doses in rodents. However, the sulfoxide group is prone to oxidation *in vivo* and a significant level of the corresponding sulfone was observed in rodent PK studies; for this reason, despite other properties being generally attractive, we discounted the sulfoxides from further progression. The sulfoximines (compounds **2**, **33** – **36** Table 5) achieved both of the key aims we set at the start of the lead optimization campaign. The *R*-stereochemistry of the sulfoximine **2** was initially inferred from the stereochemistry of the sulfoxide precursor, with imination to the sulfoximine proceeding with retention of configuration, and later confirmed from an X-ray structure (Figure 1). Interestingly, hydrogen bonds are observed only between the azaindole substituents of adjacent molecules for **2**, whereas the indole NH donor in the structure of **1** does not form a hydrogen bond. The centrosymmetric packing characteristic for methylsulfones as seen for **1** is prevented in the structure of **2** by introduction of the sulfoximine (Figure 1).

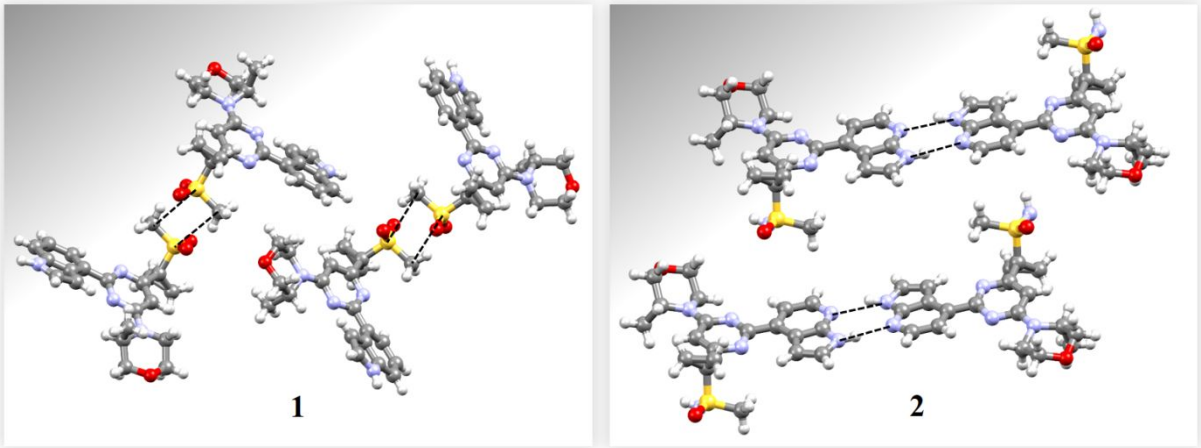

Figure 1. Small-molecule crystal structures of **1** and **2**. Short contacts of sulfonomethyl (left-hand panel) and azaindole (right-hand panel) moieties are indicated by dotted lines.

The *R*-isomer of the sulfoximine group showed slight but consistent greater potency than the corresponding *S*-isomer (compare **2** with **33**, Table 5) and similar magnitude compared with the corresponding sulfone. The sulfoximines also benefit from a significant reduction in lipophilicity and greatly improved aqueous solubility compared to the sulfones. Data from molecular matched pairs clearly show consistent retention of ATR cellular potency for the *R*-isomer, concomitant reduction in lipophilicity and improved solubility of sulfoximine analogues compared with the corresponding sulfones (Figure 2). While the sulfoximine shows a different solid-state structure, the melting point of sulfoximine **2** was measured at 222 °C and is similar to sulfone **1** (204 °C). Therefore, the observed improvement in solubility appears to be driven mainly through reduced lipophilicity, though we speculate that solvation and the removal of the methylsulfones' centrosymmetric organization may contribute additional effects which are difficult to quantify. Replacement of methylsulfones has been shown to improve solubility in other contexts,[43] and sulfoximines may have wider utility in such cases. A further lipophilicity-related benefit of the sulfoximine group was realized in reduced hERG activity and was particularly advantageous for the 2-*N*-methylamino benzimidazole analogues **35** and **36** (Figure 2). Several reviews on the properties of the sulfoximine moiety in drug

discovery have since appeared elsewhere which observe the same broad trends as described here.[44-46]

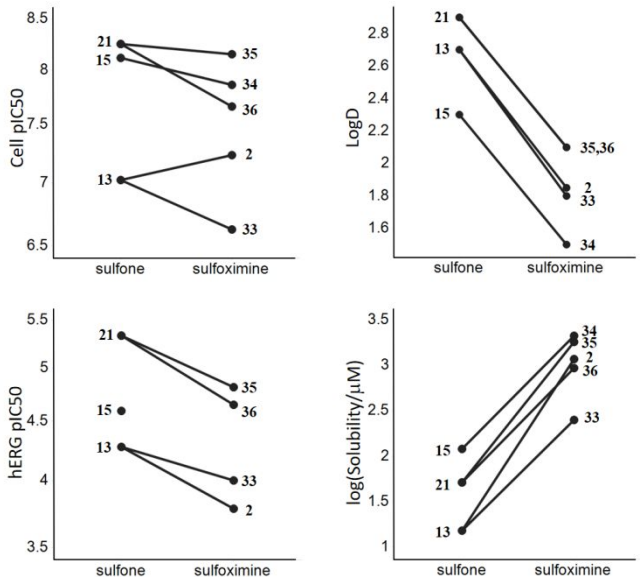

Figure 2. Sulfone and sulfoximine matched-pairs. Data for a) ATR cell pIC50; b) LogD7.4; c) hERG pIC50 and d) aqueous solubility. Numbers refer to the compounds shown in Tables 2 – 5.

Compounds that addressed the dual risks of low solubility and CYP3A4 TDI activity were further characterized as a shortlist to identify a candidate molecule for clinical-enabling studies. Physicochemical and ADME properties of compounds **2**, **15**, **21** and **35** are presented in Table 6.

Table 6. Physicochemical and ADME characterization for preclinical candidate shortlist compared with lead **1**

	1	**2**	**15**	**21**	**35**
$LogD_{7.4}$	2.5	1.9	2.1	2.8	2.1
Solubility pH7.4 (μM)[a]	10	661	108	49	>780
PPB mouse, hu (%free)[b]	14, 9.2	54, 26	48, 26	4.4, 2.2	15, 4.3
CYP3A4 IC_{50} (μM)[c]	>10	>10	>10	>10	>10
CYP3A4 %TDI, 10 μM	50	<20	<20	<18	<20
hERG IC_{50} (μM)[d]	50	166	15[†]	4.6	15
Caco-2 P_{app} A-B (pH6.5, 7.4)[e]	23, 37	6.8, 12	8, -	-, 53	-, 8
Rat, hu CL_{int}[f]	25, <3	<3.5, <3	10, <3	25, <3	11, <3
Rat AUC (μM.hr)[g]	1.0	0.8	0.08	0.4	0.35

[a] Lowest solubility result is given in the table where multiple measurements were taken: N=5 for compound **1**, N=3 for compound **15**, N=2 for compound **21**, N=7 for compound **2**; N=2 for compound **35**. [b] Measured in 10% plasma; % free calculated for 100% plasma assuming a single-site binding model. [c] >10 μM against 1A2, 2C19, 2C9, and 2D6. [d] Average activity against the human ether-a-go-go-related gene (hERG) encoded potassium channel was determined using automated whole-cell electrophysiology.[47] [e] Median A to B P_{app} (1×10^{-6} cm/s), 10 μM compound concentration. [f] Median CL_{int}: intrinsic clearance from hepatocytes (μL/min per 1×10^6 cells, 1 μM compound concentration). [g] Plasma exposure; data normalised to 1 μmol/kg; compounds were dosed orally to male Han–Wistar rats at either 4 (compounds **1** and **15**) or 10 (compounds **21**, **2** and **35**) μmol/kg formulated in propylene glycol; compounds **1**, **2**, **15**, **35** were dosed as solutions and compound **21** as a suspension. [†] The most potent of 3 measurements is shown.

All compounds have equivalent or improved cellular potency combined in most cases with reduced lipophilicity relative to the lead **1**. The sulfoximines in particular have very high aqueous solubility, high unbound fraction and none of this set of compounds exhibited CYP3A4 reversible inhibitory or TDI activity against the five major human P450 isoforms. The benzimidazole sulfone **21** has the highest lipophilicity and hERG potency. Employment of the

sulfoximine group effectively reduces lipophilicity and the hERG potency (compare sulfoximine **35** with the sulfone **21**) but without impact on ATR cellular potency. All compounds exhibited high metabolic stability in human hepatocytes. The 6-azaindole sulfone (compound **15**) and sulfoximine compounds in general tend to have lower permeability compared with indole and sulfones respectively, presumably as a result of more hydrophilic character and, in the case of the sulfoximines, the introduction of an additional strong hydrogen bond donor. However, permeability of all compounds measured in Caco-2 cells was high and each of the compounds had favorable free exposure relative to potency in rats. The 6-azaindole sulfone **15**, has the lowest total AUC. However, this is negated by a high free fraction and high cellular potency. In comparison, the sulfoximine **2** has high total exposure combined with high unbound fraction that results in very high unbound exposure.

Kinase biochemical screening at a concentration of 1 μM suggests a high level of selectivity for these optimized morpholinopyrimidine ATR inhibitors. Kinome selectivity is depicted in Figure 3 for sulfoximine **2** (the graphs for 2-aminobenzimidazole sulfone **21** and 6-azaindole sulfone **15** in comparison to the aminopyrazine **3** can be found in the Supplementary Materials Figure S1). Compound **2** showed excellent selectivity, with inhibition of ~60% for PIK3C2G and CLK4 (at 1 μM), and <50% inhibition for the remaining 407 kinases tested (data supplied in Supplementary Materials). The PI3K and PIKK-family specificity for the morpholinopyrimidine ATR inhibitors is shown in Table 7.

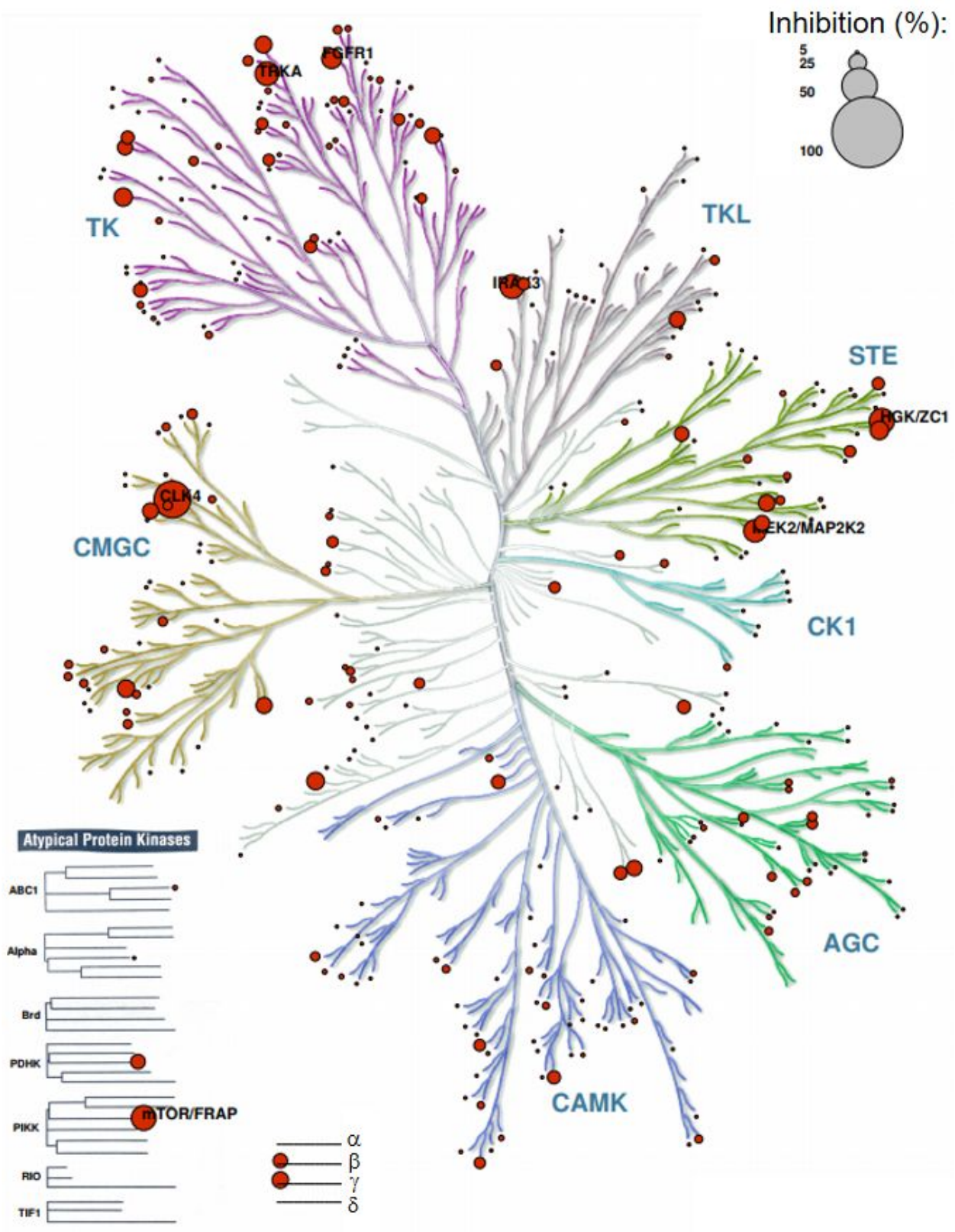
Inhibition (%):
5
25
50
100
TK
TKL
STE
CMGC
CK1
AGC
CAMK
TRKA
PGFR1
IRAK3
RGK/ZC1
CLK4
MEK2/MAP2K2
Atypical Protein Kinases
ABC1
Alpha
Brd
PDHK
PIKK
mTOR/FRAP
RIO
TIF1
α
β
γ
δ

Figure 3. Kinome selectivity depiction for compound **2**. Inhibition data (%) shown for a compound test concentration of 1 μM. PI3K isoforms indicated as α, β, γ, δ. Data in Supplementary Materials, Table T1.

Table 7. PI3K, PIKK-family selectivity and growth inhibitory potency for preclinical candidate shortlist compared with lead **1**

	1	**2**	**15**	**21**	**35**
ATR Cell IC_{50} (μM)[a]	0.061	0.074	0.012	0.008	0.009
mTOR IC_{50} (μM)[b]	0.038	0.37	0.034	0.052	0.15
mTOR cell: AKT pS473 IC_{50} (μM)[c]	2.4	>23	1.4	4.0	9.8
mTOR cell: p70S6K S235/236 IC_{50} (μM)[d]	0.72	5.7	0.27	1.5	3.1
PI3Kα cell IC_{50} (μM)[e]	>30	>30	>30	.30	>30
ATM cell IC_{50} (μM)[f]	>30	>30	>30	>30	>30
DNA-PK cell IC_{50} (μM)[g]	>30	>30	>30	>30	>30
LoVo GI_{50} (μM)[h]	0.20	0.44	0.056	0.10	0.25
HT29 GI_{50} (μM)[h]	0.97	2.6	0.31	0.55	1.2

[a] See footnote of Table 1. [b] Standard error of mean (SEM) pIC_{50} measurement is ≤0.13. [c] Inhibition of AKT pSer473 in MDA-MB-468 cells. [d] Inhibition of p70S6K pSer235/236 in MDAMB-468 cells. [e] Inhibition of pAKT T308 in BT-474 cells. [f] Inhibition of ATM Ser1981 in HT-29 cells following IR treatment. [g] Inhibition of DNA-PK pSer2056 in HT-29 cells following IR treatment. [h] MTS (tetrazolium dye) assay with 72 h continuous exposure to compounds.

The 2-aminobenzimidazole **21** and 6-azaindole sulfone **15** also display excellent selectivity over all kinase classes but have a degree of promiscuity versus lipid kinases. It is interesting to compare kinase selectivity with the aminopyrazine **3** which exhibits a wholly different profile, something that is not unexpected given that it belongs to a different structural class (see Supplementary Materials Figure S1). The aminopyrazine **3** has been reported to have high ATR

specificity particularly over the closely related mTOR.[48] The morpholinopyrimidine inhibitors were also screened specifically for inhibition of the related targets mTOR, PI3Kα, ATM and DNA-PK. These compounds all show moderate inhibitory potency, relative to ATR, against mTOR in an enzyme assay and some activity in cell assays reading out mTORC1 (inhibition of AKT pSer473) and mTORC2 (inhibition of p70S6K pSer235/236). This is unsurprising as the PI3K and PIKK kinases are known to have similar binding sites, with some compounds such as NVP-BEZ235,[6] exhibiting a promiscuous pan-PI3K and -PIKK profile. In terms of protein sequence similarity, mTOR and ATM are nearest neighbors of ATR, yet, a margin of activity was observed in all cases including mTOR, relative to inhibition of ATR-dependent kinase signaling. Moreover, no activity could be detected for PI3Kα, ATM or DNA-PK in cell-based systems. These combined data suggest the optimized compounds are unlikely to have activity against other PI3K/PIKK signaling pathways at relevant doses. LoVo are MRE11A-mutant (MRE11A is key component of the ATM signaling and DNA double-strand break (DSB) repair pathway) colorectal adenocarcinoma cells which are sensitive to ATR inhibitors.[16] Compound **1** was shown to induce S-phase arrest, an increase in γH2AX over time and caspase-3 activation and cell death.[49] HT29 colorectal adenocarcinoma cells are classified as MRE11A and ATM-proficient expressing high levels of total ATM protein without an ATM pathway defect and therefore expected to be relatively insensitive to selective ATR inhibition. As can be seen in Table 7, the morpholinopyrimidine ATR inhibitors show greater growth inhibition in LoVo compared with HT29 in support of this general hypothesis. Across a broader cell panel, ATR inhibitors from structurally orthogonal series show an inhibition profile that is distinct from

PI3K and PIKK-family inhibitors, further supporting a cellular mode of action arising from selective ATR inhibition (Figure 4).

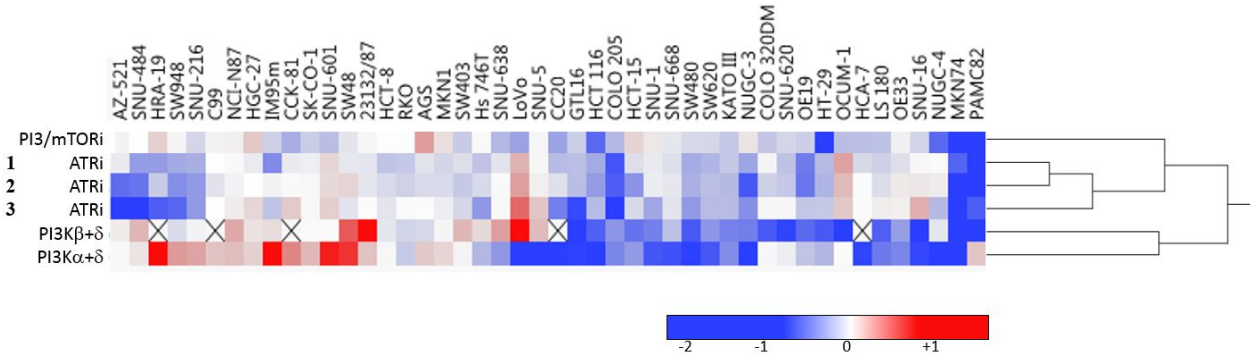

Figure 4. Colon and gastric tumor cell line responses for ATR inhibitors **1**, **2**, **3** compared with: NVPBEZ-235 (labelled pPI3/mTORi)[6] (mTOR, PI3K, ATR, ATM, DNA-PK), AZD8186[50] (labelled PI3Kβ+δ) and AZD8835[51] (labelled PI3K α+δ). Data shown is normalised as pGI50 minus mean pGI50 across the panel to correct for the influence of absolute potency. Hierarchical clustering of profiles is shown on the right.

The compounds were next characterized for tumor growth inhibition (TGI) *in vivo*. Compounds were first administered at their maximum well-tolerated daily dose by oral gavage to female nude mice bearing human LoVo colorectal adenocarcinoma xenografts. Mouse tolerance of the morpholinopyrimidine ATR inhibitors was found to be variable. Indole sulfone **1** and the sulfoximines **2** and **35** were well tolerated at 50 mg/kg once daily (QD) whereas the 6-azaindole sulfone **15** and 2-methylaminobenzimidazole sulfone **21** were

tolerated at a maximum daily dose of 25 mg/kg QD. From a mechanistic standpoint and as a monotherapy, we expected continuous exposure would be required to drive efficacy.[16] A broad relationship can be seen between the observed tolerance, efficacy and compound exposure in mouse relative to potency.

Table 8. Monotherapy *in vivo* tumor growth inhibition (TGI) in human LoVo colorectal adenocarcinoma xenografts.

Compound	Dose (mg/kg)	Schedule	TGI[a] (p-value T-test vs. vehicle control)
1	50	QD, 20 d	88 (p<0.0005
	50	QD, 14 d	67 (p<0.0005)
	50	QD, 13 d	77 (p<0.0005)
	25	BD, 13 d	78 (p<0.0005)
2	75	QD, 11 d	>100 (p<0.0005)
	50	QD, 14 d	72 (p<0.0005)
	50	QD, 13 d	81 (p<0.0005)
	50	QD, 15 d	89 (p<0.0005)
	25	QD, 15 d	38 (p<0.049)
	25	QD, 11 d	45 (p<0.002)
	10	QD, 15 d	7 (p *ns*)
	25	BD, 13 d	96 (p<0.0005)
	12.5	BD, 11 d	45 (p<0.0002)
15	25	QD, 20 d	60 (p<0.0005)
	25	QD, 13 d	59 (p<0.0005)
	12.5	BD, 13 d	62 (p<0.0005)
21	25	QD, 20 d	67 (p<0.0005)
35	50	QD, 14 d	27 (p<0.05)

[a] Female nude mice bearing established human LoVo xenografts were dosed orally with compound at the indicated dose and schedule. ns = not significant

Table 9. Plasma concentration at 8 hours following multiple doses in nude mouse at compound maximum well tolerated dose.

Compound	Dose (mg/kg)	Dosing frequency	Mean 8 h plasma concentration, μM (Std Dev)[a]	Free plasma LoVo multiple
1	50	QD	3.5 (1.2)	2.5
	25	BD	1.8 (0.62)	1
2	75	QD	2.6 (2.0)	3
	50	QD	2.2 (0.52)	3
	25	BD	0.74 (0.58)	1
15	25	QD	0.78 (0.62)	6.5
	12.5	BD	0.22 (0.20)	2
21	25	QD	8.3 (1.3)	3.5
35	50	QD	0.94 (0.39)	0.5

[a] Female nude mice bearing established human LoVo colorectal adenocarcinoma xenografts were dosed orally with compounds either once-daily (QD) [compound **1**: averaged data from 3 {N=10, mean=4.2 μM (Std Dev=1.3)}, 4 {N=10, 3.1 (1.1)} and 14 {N=10, 3.2 (0.77)} consecutive doses; compound **2**: 75 mg/kg: averaged data from 4 doses, 50 mg/kg: averaged data from 4 {N=5, 2.1 (0.65)}, and 14 {N=10, 2.3 (0.49)}, consecutive doses; compound **15**: 4 consecutive doses (N=10 independent samples); compound **21**: 4 consecutive doses (N=5 independent samples); compound **35**: 14 consecutive doses (N=10 independent samples)] or twice-daily for 8 consecutive doses. Plasma was sampled at 8 hours following the last dose.

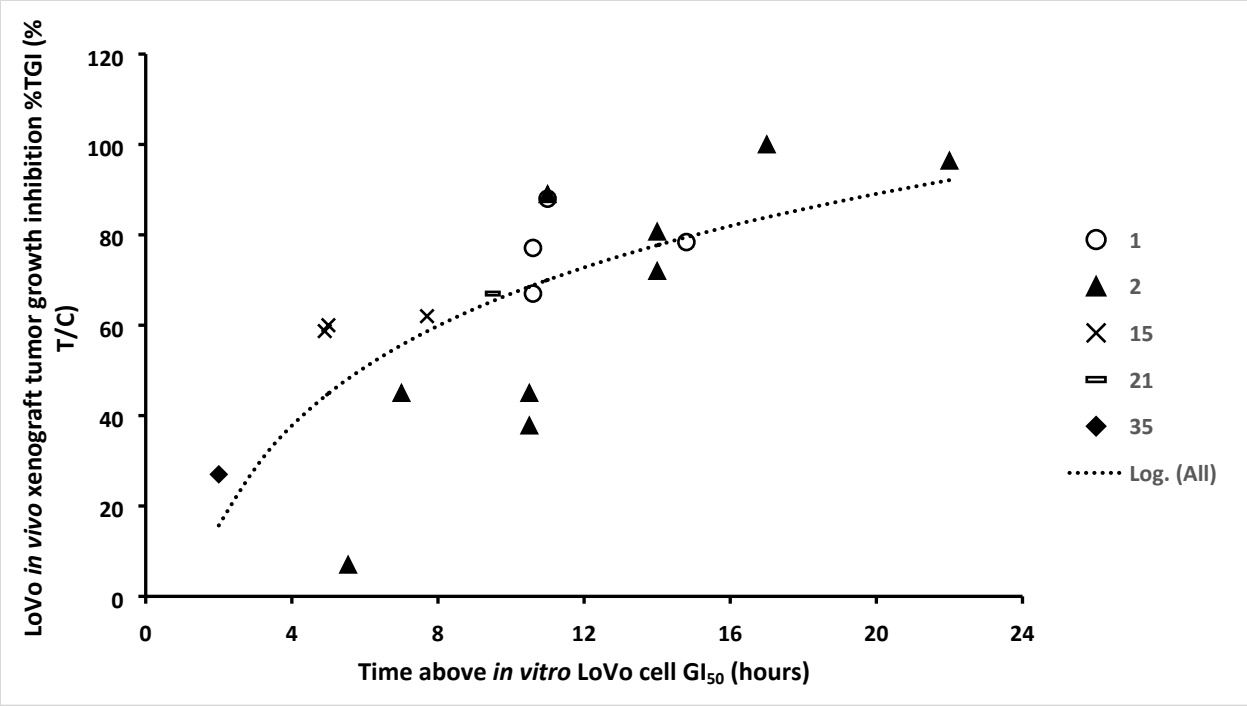

Figure 5. Exposure of ATR inhibitors **1**, **2**, **15**, **21**, and **35** is correlated to tumor growth inhibition (TGI). The observed plasma concentrations following a single dose of each compound were multiplied by the compound specific *in vitro* measured free fraction and divided by *in vitro* GI_{50} to give fold free concentration above GI_{50}. The time above *in vitro* LoVo GI_{50} is plotted against LoVo xenograft tumor growth inhibition *in vivo*. A logarithmic trendline (Log.(All)) best-fit curve is shown for all compounds.

All compounds other than compound **35**, achieved TGI >50% in the LoVo model when dosed once daily over the course of the study (Table 8). The comparative lack of efficacy for compound **35** can be explained by the lowest free plasma concentration multiple over LoVo

GI_{50} measured at 8 h of all the compounds tested (Table 9). The 7-azaindole sulfoximine **2** showed the greatest TGI, equivalent or greater at 50 mg/kg across multiple experiments, to the indole sulfone lead **1** and this is associated with free plasma concentration at 8 h in excess of the LoVo GI_{50}. The total plasma concentration of the 6-azaindolesulfone **15** was found to be the lowest of the compounds tested but the combination of high unbound fraction with high potency results in a high free plasma multiple over LoVo GI_{50}. In contrast, benzimidazole sulfone **21** shows high total drug plasma concentration and high potency but has a relatively high bound fraction, particularly in comparison to compounds **2** and **15**, and this leads to a free plasma multiple over LoVo GI_{50} in a similar range to the other compounds. Twice-daily dosing was investigated for compounds **1**, **2** and **15** in an attempt to achieve longer exposure and drive a greater tumor response. When the maximum well-tolerated daily single dose was split (dosed 8 hour apart), neither compound **15** or **1** showed greater anti-tumor activity. For indole sulfone **1**, this may be explained by a relatively flat PK profile in the mouse negating the impact of twice daily dosing (BD).[16] The 6-azaindole sulfone **15** has a relatively short half-life in mouse and we expected BD dosing would lead to greater efficacy. However, the efficacy achieved for compound **15** dosed BD was indistinguishable from the higher single dose. In contrast, 7-azaindole sulfoximine **2** achieved near complete TGI in the LoVo xenograft model when administered at a dose of 25 mg/kg BD. The time each day that free concentrations in plasma were above the *in vitro* LoVo GI_{50} was estimated using the observed plasma concentrations following a single dose of each compound. This duration exhibits a saturating relationship with tumor growth inhibition (Figure 5). The relationship is consistent across compounds

regardless of differences in pharmacokinetic properties, including different terminal half-lives in the mouse. This analysis broadly correlates with the cover seen in earlier experiments, with **15** showing the largest difference. A clear dose-response could be demonstrated for **2** in LoVo (Table 8 and Figure 6, top graph) and this was compared with HT29 (Figure 6, bottom graph). Compound **2** delivers significant TGI in LoVo at doses as low as 25 mg/kg QD or 12.5 mg/kg BD. A dose of 75 mg/kg QD leads to regression in the LoVo model albeit tolerability is borderline with 4 of 10 animals in the group terminated in accord with study protocol due to bodyweight loss greater than 15%. In the remaining six animals a maximum bodyweight loss of 9% was observed. Therefore 75 mg/kg, while formerly tolerated, was not considered to be a well-tolerated dose. The observed *in vitro* sensitivity (Table 7) translated *in vivo* with no significant anti-tumor efficacy observed for **2** in HT29 using doses and schedules which are highly active in LoVo xenografts (Figure 6, bottom graph). γH2AX is a sensitive marker for DNA damage and a useful marker to study ATR inhibition. Increases in γH2AX reflect the time- dependent accumulation of collapsed replication forks, which only occur in actively replicating cells during S-phase of the cell cycle), and replication-associated DSBs.[52, 53] In LoVo xenografts, the magnitude and maintenance of γH2AX over 24 hours is obtained in a dose-dependent manner after repeat daily dosing with the sulfoximine **2** (Figure 7) and this is associated with the greater anti-tumor effect observed for this compound. We observe an indirect relationship between plasma PK and tumor PD based on γH2AX induction, with signals being sustained beyond 24 hours despite plasma concentrations predicted to be below detectable levels at this timepoint (LOQ 0.09 μM data not shown). While we need sufficient

levels and duration of cover to induce DNA breaks and γH2AX, once these have formed it may take many hours for the damage to be repaired, or cells to die, and the γH2AX signal to dissipate. Persistence of γH2AX signal over time (after the damage insult) is indicative of unrepaired DSBs and/or DNA repair inhibition and is observed even after breaks have been repaired.[52]

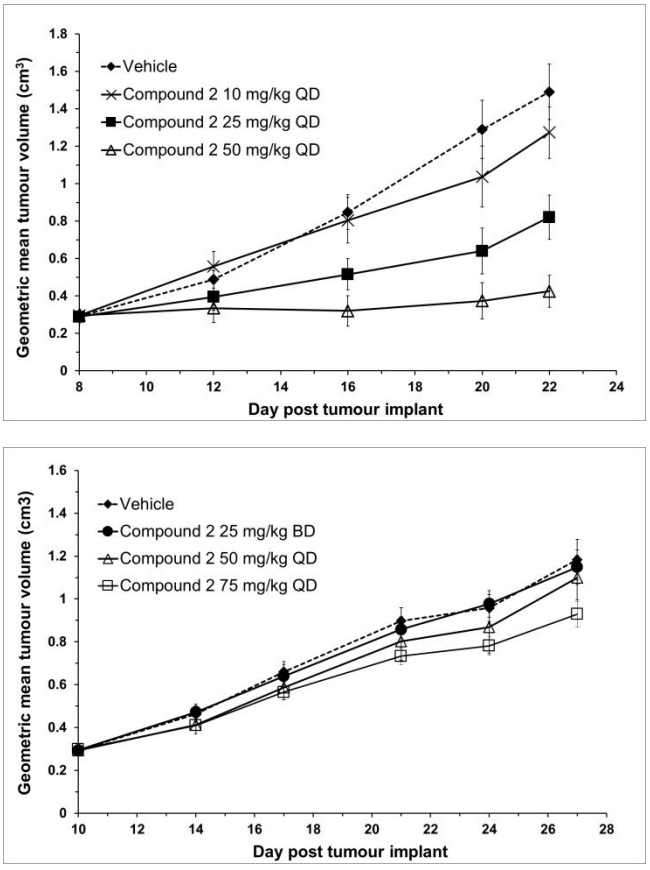

Figure 6. *In vivo* tumor growth inhibition (TGI) for compound **2**. Top graph: female nude mice bearing established human LoVo (MRE11A mutant/ATM deficient) colorectal adenocarcinoma xenografts were dosed orally with either vehicle (♦) or **2** at 10 mg/kg once

daily (×, day 22 TGI = 7%, p= ns), 25 mg/kg once daily (■, day 22 TGI = 38%, p<0.049), 50 mg/kg once daily (△, day 22 TGI = 89%, p<0.0005). Bottom graph: female nude mice bearing established HT-29 (MRE11A wild type/ATM-proficient) colorectal adenocarcinoma xenografts were dosed orally with either vehicle (♦) or **2** at 25 mg/kg twice daily (●, day 27 TGI = 5%, p= ns), 50 mg/kg once daily (△, day 27 TGI = 10%, p= ns) or 75 mg/kg once daily (□, day 27 TGI = 30%, p<0.005); ns = not significant.

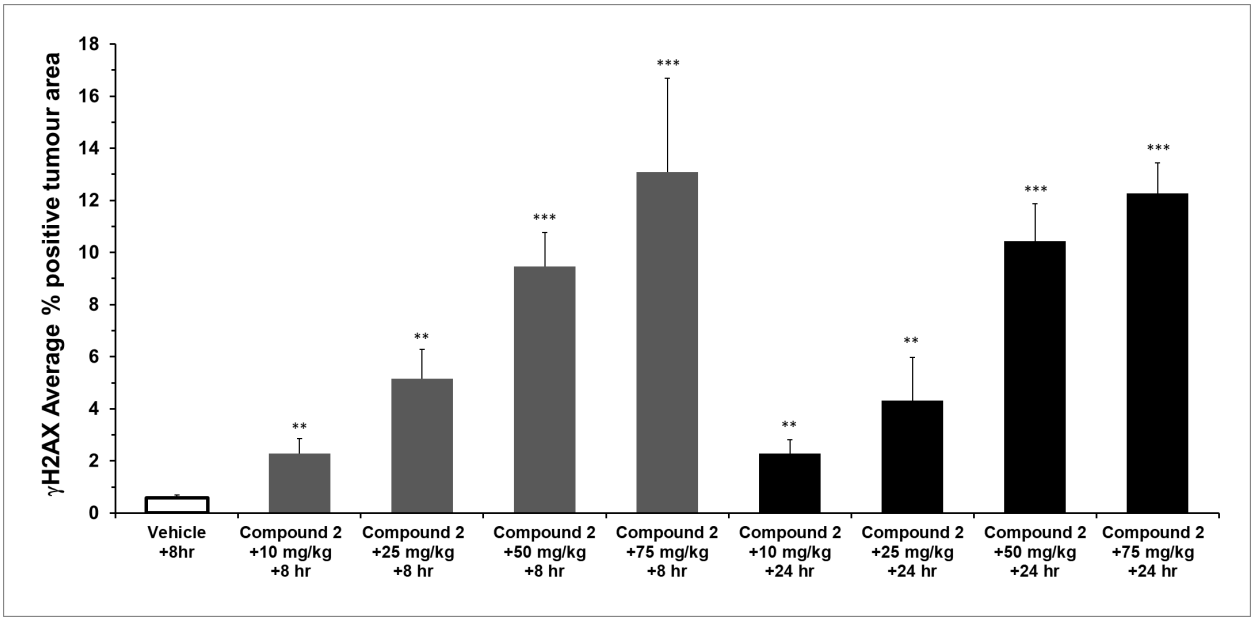

Figure 7. Compound **2** γH2AX DNA-damage biomarker pharmacodynamics in established LoVo tumor xenografts in female nude mice. Mice were dosed with either vehicle or **2** at 10 mg/kg, 25 mg/kg, 50 mg/kg or 75 mg/kg once daily for 4 consecutive days before tissue sampling at 8 hours or 24 hours after the 4th dose (day 4). Data are presented as average %

γH2AX positive tissue per total tumor area counted ± Standard Deviation (n=4 independent mouse/tumors per point).

Compound **2** has highly attractive physicochemical properties with a low biopharmaceutical risk profile (Table 10). For completeness we examined the methylmorpholine stereoisomers of compounds **2** and **33** and prepared the 3(*S*)-methylmorpholine matched pairs (compounds **37** and **38** respectively, Table S2 Supplementary Materials) and these were found to have significantly reduced potency as would be predicted from the described SAR. A stable crystalline form of **2** possesses high solubility in aqueous and biorelevant media such as Simulated Gastric Fluid (SGF) and Fasted State Simulated Intestinal Fluid (FaSSIF) (Table 10). Pharmacokinetic evaluation of **2** shows this compound has low to moderate clearance, moderate volume of distribution and good bioavailability in rodent and dog. Physiologically based pharmacokinetic (PBPK) modelling,[54, 55] using *in vitro* and *in vivo* data across preclinical species, predicts **2** to have low human clearance (average clearance of 1.98 mL/min/kg) and estimated volume of distribution of 1 L/kg leading to a terminal half-life of 6 hours in man. *In silico* modelling of human absorption,[56] predicts compound **2** will have high bioavailability (~80%) and a maximum absorbable dose D_{abs},[25, 57] of ~2,500 mg. The preclinical TGI data for compound **2** and related compounds suggests that the duration of free drug exposure is correlated with monotherapy efficacy. A PK/PD model was created linking the preclinical pharmacokinetics of **2** with the DNA-damage biomarker γH2AX and tumor growth inhibition

in the LoVo xenograft model. Simulations using the monotherapy LoVo GI_{50} as the target unbound trough concentration led to a predicted efficacious dose in human[58] of 200 mg (unbound C_{max} = 0.93 μM) dosed BD assuming continuous exposure is required across the full dose interval. While it is likely that target drug concentration and/or duration will be lower when ATR inhibitors are dosed in combination, dose prediction based on monotherapy pharmacodynamic modulation and efficacy provides a reasonable basis to estimate the efficacious dose in man. The monotherapy human dose estimate is well below the calculated D_{abs}, and therefore **2** has low risk of requiring development of an enabling formulation for use in the clinic, whether used alone or in combination. The profound anti-tumor activity and associated pharmacodynamics combined with favorable dose estimate and pharmaceutical properties led to the sulfoximine **2** being selected for IND-enabling studies and subsequently this compound became AZD6738.

Table 10. Physicochemical properties, preclinical PK and predicted human PK and dose of **2**

	2
Estimated p*K*a	3.8 (B1) 2.2 (B2)
Solubility SGF pH2.5, FaSSIF pH6.5 (mg/mL)	26.7, 0.49
Rat PK[a]: Cl, %LBF / Vd_{ss}, L/kg / bioavailability, %	22 / 3.1 / 67
Dog PK[b]: Cl, %LBF / Vd_{ss}, L/kg / bioavailability, %	10 / 1 / 100
Hu CL_{int}[c]	2.0
Predicted hu PK: Cl, %LBF / Vd_{ss}, L/kg / bioavailability, % / T1/2, h	11 / 1.0 / 80 / 6

Maximum absorbable dose (D_{abs})[d]	2492
Predicted hu dose (mg)[e]	200

[a] Rat plasma PK in male Han Wistar rats, dosed at 8.55 (IV) and 20.3 (PO) μmol/kg. [b] Dog blood PK in male and female Beagle dogs, dosed at 10.5 (IV) and 15.1 (PO) μmol/kg. [c] Estimate of median intrinsic clearance obtained from hepatocyte data using intercept method[59] (μL/min per 1 x 10^6 cells, 1 μM compound **2**. [d] Maximum absorbable dose (D_{abs}).[25] [e] Predicted human dose assuming trough concentration = 0.43 μM dosed BD.

Compound **2** (AZD6738) has progressed into human clinical trials and is being assessed in multiple Phase I/II studies as a monotherapy and in combination with carboplatin (NCT02264678), paclitaxel (NCT02630199), radiotherapy (NCT02223923), and the novel agents olaparib (NCT03462342, NCT03330847), acalabrutinib (NCT03328273) and durvalumab (NCT03334617). Plasma pharmacokinetics in man showed rapid absorption of compound **2**, with peak plasma concentration at ~1.5 hours post-dose, and a biphasic decline with an elimination half-life of 11.0 hours; and despite ~45% variability in clearance, there was dose proportionality to at least 320 mg QD.[60, 61] Plasma pharmacokinetics aligned well with target preclinical free drug exposure and duration, with cover over ATR cell IC_{90} obtained in ≥50% of patients with a 80-320 mg daily dose range (QD). The observed levels are expected to drive significant ATR inhibition, with cover increased in a dose dependent manner up to ATR IC_{96}.[62] Preclinical work has demonstrated further potential for combination therapy with e.g. olaparib[63]. Early data from dose escalation studies with combination partners olaparib and durvalumab was presented recently[61] showing good tolerance for compound **2** in combination

dose escalation, and preliminary signals of anti-tumor activity, with no evidence of drug-drug-interactions (DDI); in 44 patients treated at various doses of compound **2** (60 mg through 240 mg QD) in combination with olaparib, 1 RECIST complete response (CR) and 6 partial responses (PR; 1 unconfirmed) were observed in patients with BRCA1 or BRCA2 mutations independent of ATM status, in advanced breast (3 patients), and 1 each of ovarian, prostate, pancreatic and ampullary cancer; and in 25 patients treated at various doses (80 mg through 240 mg BD) in combination with durvalumab, 1 RECIST CR and 3 PRs, in patients with advanced NSCLC (3 patients) and HNSCC (1 patient), independent of tumor PD-L1 expression were observed.[61]

CONCLUSIONS

ATR plays a key role in DNA-damage repair, and only recently highly potent and selective compounds have entered clinical assessment. Here we report the discovery of **2** (AZD6738), an inhibitor of ATR currently being examined in Phase I/II clinical trials. Starting from a lead compound containing a sulfone group and substitution with a sulfoximine moiety led to **2**, a compound with excellent solubility, good cell potency and high selectivity across the kinome.

The promising preclinical data package for compound **2** combined with moderate predicted human dose strongly supported its selection as a clinical candidate. First dose of compound **2** in patients was achieved in 2013. Pharmacokinetics in man was found to be dose-dependent with efficacious exposure in alignment with the preclinical prediction together with promising early signs of clinical efficacy.[8, 61] AZD6738 is currently in multiple Phase II studies as a

monotherapy and in combination with carboplatin (NCT02264678), paclitaxel (NCT02630199), radiotherapy (NCT02223923), and the novel agents olaparib (NCT03462342, NCT03330847), acalabrutinib (NCT03328273) and durvalumab (NCT03334617).

EXPERIMENTAL SECTION

General Synthetic Methods. All experiments were carried out under an inert atmosphere and at room temperature (rt) unless otherwise stated. Microwave reactions were performed using either the Biotage initiator or CEM Explorer. Workup procedures were carried out using traditional phase separating techniques or by using strong cation exchange (SCX) chromatography using Isolute SPE flash SCX-2 column (International Sorbent Technology Limited, Mid Glamorgan, U.K.). When necessary, organic solutions were dried over anhydrous $MgSO_4$ or Na_2SO_4. Flash column chromatography (FCC) was performed on Merck Kieselgel silica (article 9385) or on Silicycle cartridges (40–63 μm silica, 4–330 g weight) or on GraceResolv cartridges (4–120 g) either manually or automated using an Isco Combi Flash Companion system. Preparative reverse phase HPLC (RP HPLC) was performed on C18 reversed-phase silica, for example, on a Waters "Xterra" or "XBridge" preparative reversed-phase column (5 μm silica, 19 mm diameter, 100 mm length) or on a Phenomenex "Gemini" or "AXIA" preparative reversed-phase column (5 μm silica, 110A, 21.1 mm diameter, 100 mm length) using decreasingly polar mixtures as eluent, for example, containing 0.1% formic acid or 1% aqueous ammonium hydroxide (d = 0.88) as solvent A and acetonitrile as solvent B. The

following preperative chiral HPLC methods were used; in general a flow rate of between 10-350 mL/min and detection was by UV absorbance at a typical wavelength of 254 nm. A sample concentration of about 1-100 mg/mL was used in a suitable solvent mixture such as MeOH, EtOH or iPA optionally mixed with *iso*-hexane or heptane with an injection volume of between 0.5-100 mL and run time of between 10-150 min and a typical oven temperature of 25-35 ˚C. The following analytical chiral HPLC methods were used; in general a flow rate of 1 mL/min and detection was by UV absorbance at a typical wavelength of 254 nm. A sample concentration of about 1 mg/mL was used in a suitable solvent such as EtOH with an injection volume of about 10 μl and run time of between 10-60 min and typical oven temperature of 25-35 ˚C. The following preperative SFC (supercritical fluid chromotography) methods were used; in general a flow rate of about 70 mL/min and detection was by UV absorbance at a typical wavelength of 254 nm. A sample concentration of about 100 mg/mL was used in a suitable solvent such as MeOH with an injection volume of about 0.5 mL and run time of between 10-150 min and typical oven temperature of 25-35 ˚C. Intermediates were not necessarily fully purified, but their structures and purity were assessed by TLC, NMR, HPLC, and mass spectral techniques and are consistent with the proposed structures. The purities of compounds for biological testing were assessed by NMR, HPLC, and mass spectral techniques and are consistent with the proposed structures; purity was ≥95%. Electrospray mass spectral data were obtained using a Waters ZMD or Waters ZQ LC/mass spectrometer acquiring both positive and negative ion data, and generally, only ions relating to the parent structure are reported. Unless otherwise stated, ^{1}H NMR spectra were obtained using a Bruker DRX400 operating at

400 MHz in DMSO-d6 or $CDCl_3$. Chemical shifts are reported as δ values (ppm) downfield from internal TMS in appropriate organic solutions. Peak multiplicities are expressed as follows: s, singlet; d, doublet; dd, doublet of doublet; t, triplet; br s, broad singlet; m, multiplet. Analytical HPLC was performed on C18 reverse-phase silica, on a Phenomenex "Gemini" preparative reversed-phase column (5 μm silica, 110A, 2 mm diameter, 50 mm length) using decreasingly polar mixtures as eluent, for example, decreasingly polar mixtures of water (containing 0.1% formic acid or 0.1% ammonia) as solvent A and acetonitrile as solvent B or MeOH/MeCN, 3:1, with a flow rate of about 1 mL/min, and detection was by electrospray mass spectrometry and by UV absorbance at a wavelength of 254 nm. Accurate mass spectra were recorded on a Themo LTQ-FT in +ve ion mode with a Thermo Accela pump and Surveyor PDA+ with a CTC autosampler, and the results agreed with the theoretical values to within 4 ppm. Combustion analyses (C, H, N) were performed with a Carlo Erba EA1108 analyzer, and the results agreed with the theoretical values to within ±0.5%. Water was measured by the Karl Fischer method using a Mettler DL 18. Where the synthesis of an intermediate or reagent is not described it has either been described in the literature previously or is available from commercial sources.

4-{4-[(3*R*)-3-Methylmorpholin-4-yl]-6-[1-((*R*)-*S*-methylsulfonimidoyl)cyclopropyl]pyrimidin-2-yl}-1*H*-pyrrolo[2,3-*b*]pyridine (2). Bis(triphenylphosphine)palladium(II) chloride (27.5 g, 39.14 mmol) was added to a suspension of **R-75** (259 g, 782.87 mmol), 1*H*-pyrrolo[2,3-*b*]pyridin-4-ylboronic acid (152 g, 939.45 mmol)

and sodium carbonate (2M aq.) (1174 mL, 2348.61 mmol) in degassed DME:H2O (4:1) (2740 mL) and stirred to 90 °C for 60 min. A further portion of 1*H*-pyrrolo[2,3-*b*]pyridin-4-ylboronic acid (15.2 g, 93.95 mmol) was added and the reaction stirred for another 60 min. The reaction mixture was diluted with EtOAc (200 mL) and washed with water (200 mL). The organic layer was dried over $MgSO_4$, filtered and then concentrated *in vacuo*. The crude product was purified by flash chromatography on silica, eluting with a gradient of 0 to 10 % MeOH in EtOAc. Pure fractions were evaporated to dryness to afford a cream foam. MTBE (2500 mL) was added and the mixture stirred at room temperature for 3 days before the solid was isolated by filtration to afford **2** (139 g, 42%) as a white crystalline solid. ^{1}H NMR (400 MHz, DMSO-d6): 1.19 (3H, d), 1.29 - 1.50 (3H, m), 1.61 - 1.72 (1H, m), 3.01 (3H, s), 3.22 (1H, d), 3.43 (1H, td), 3.58 (1H, dd), 3.68 - 3.76 (2H, m), 3.87 - 3.96 (1H, m), 4.17 (1H, d), 4.60 (1H, s), 6.98 (1H, s), 7.20 (1H, dd), 7.55 - 7.58 (1H, m), 7.92 (1H, d), 8.60 (1H, d), 11.67 (1H, s). ^{13}C NMR (176 MHz, DMSO-d6) 11.29, 12.22, 13.39, 38.92, 41.14, 46.48, 47.81, 65.97, 70.19, 101.54, 102.82, 114.58, 117.71, 127.21, 136.70, 142.21, 150.12, 161.88, 162.63, 163.20. HRMS-ESI *m*/*z* 413.17529 [MH^+]; $C_{20}H_{24}N_6O_2S$ requires 413.1760. Chiral HPLC: (HP1100 system 4, 5 μm Chiralpak AS-H (250 mm × 4.6 mm) column, eluting with *iso*-hexane/EtOH/MeOH/TEA 50/25/25/0.1) R_f = 8.252, >99%. Anal. Found (% w/w): C, 58.36; H, 5.87; N, 20.20; S, 7.55; H_2O, <0.14. $C_{20}H_{24}N_6O_2S$ requires C, 58.23; H, 5.86; N, 20.37; S, 7.77.

4-{4-[(3*R*)-3-Methylmorpholin-4-yl]-6-[1-((*R*)-*S*-methylsulfonimidoyl)cyclopropyl]pyrimidin-2-yl}-1*H*-pyrrolo[2,3-*b*]pyridine (2), and 4-{4-

[(3*R*)-3-Methylmorpholin-4-yl]-6-[1-((*S*)-*S*-methylsulfonimidoyl)cyclopropyl]pyrimidin-2-yl}-1*H*-pyrrolo[2,3-*b*]pyridine (33). Dichlorobis(triphenylphosphine)palladium(II) (0.073 g, 0.10 mmol) was added in one portion to **R/S-75** (1.383 g, 4.18 mmol), 2M sodium carbonate (aq.) (2.508 mL, 5.02 mmol) and 4-(4,4,5,5-tetramethyl-1,3,2-dioxaborolan-2-yl)-1-tosyl-1*H*-pyrrolo[2,3*b*]pyridine (1.665 g, 4.18 mmol) in DME:water 4:1 (100 mL) under nitrogen. The reaction mixture was stirred at 90 °C for 6 hours. The reaction mixture was concentrated and diluted with EtOAc (400 mL), and washed sequentially with water (300 mL) and saturated brine (75 mL). The organic layer was dried over $MgSO_4$, filtered and evaporated onto silica gel (30 g). The resulting powder was purified by flash chromatography on silica, eluting with a gradient of 0 to 5% MeOH in DCM. Pure fractions were evaporated to dryness to afford (3*R*)-3-methyl-4-(6-(1-(*S*-methylsulfonimidoyl)cyclopropyl)-2-(1-tosyl-1*H*-pyrrolo[2,3-*b*]pyridine-4-yl)pyrimidin-4-yl)morpholine (2.174 g, 92%). ^{1}H NMR (400 MHz, $CDC1_3$): 1.37 (3H, d), 1.56 (2H, m), 1.83 (2H, q), 2.37 (4H, s), 3.16 (3H, s), 3.36 (1H, td), 3.60 (1H, td), 3.74 (1H, dd), 3.85 (1H, d), 4.01 - 4.19 (2H, m), 4.49 (1H, s), 6.95 (1H, d), 7.28 (2H, d, obscured by $CDCl_3$ peak), 7.44 (1H, t), 7.82 (1H, d), 8.02 - 8.11 (3H, m), 8.52 (1H, d). MS-ESI *m/z* 567 [MH^+].

(3*R*)-3-Methyl-4-(6-(1-(*S*-methylsulfonimidoyl)cyclopropyl)-2-(1-tosyl-1*H*-pyrrolo[2,3-*b*]pyridine-4-yl)pyrimidin-4-yl)morpholine (1.67 g, 2.95 mmol) was dissolved in DME:water 4:1 (60 mL) and heated to 50 °C. 2M Sodium hydroxide (aq.) (2.58 mL, 5.16 mmol) was then added and heating continued for 18 hours. The reaction mixture was acidified with 2M HCI (~2 mL) to pH5. The reaction mixture was evaporated to dryness and the residue dissolved in

EtOAc (250 mL) and washed with water (200 mL). The organic layer was dried over $MgSO_4$, filtered and evaporated onto silica gel (10 g). The resulting powder was purified by flash chromatography on silica, eluting with a gradient of 0 to 7% MeOH in DCM. Pure fractions were evaporated and the residue was purified by preparative chiral chromatography on a Merck 50mm, 20μm ChiralCel OJ column, eluting isocratically with *iso*-hexane/EtOH/MeOH/TEA (50/25/25/0.1) as eluent. The fractions containing the desired compound were evaporated to dryness to afford **2** (0.538 g, 44%) as the first eluting compound. ^{1}H NMR (400 MHz, DMSO-d6): 1.29 (3H, d), 1.51 (3H, m), 1.70 - 1.82 (1H, m), 3.11 (3H, s), 3.28 (1H, m, obscured by water peak), 3.48 - 3.60 (1H, m), 3.68 (1H, dd), 3.75 - 3.87 (2H, m), 4.02 (1H, dd), 4.19 (1H, d), 4.60 (1H, s), 7.01 (1H, s), 7.23 (1H, dd), 7.51 - 7.67 (1H, m), 7.95 (1H, d), 8.34 (1H, d), 11.76 (1H, s). MS-ESI *m/z* 413 [MH^+]. Chiral HPLC: (HP1100 System 4, 5μm Chiralcel OJ-H (250 mm x 4.6 mm) column eluting with *iso*-hexane/EtOH/MeOH/TEA (50/25/25/0.1) Rf, 9.013 >99%; and **33** (0.441 g, 36%) as the second eluting compound. ^{1}H NMR (400 MHz, DMSO-d^6) 1.28 (3H, d), 1.40 - 1.58 (3H, m), 1.70 - 1.80 (1H, m), 3.10 (3H, d), 3.23 - 3.27 (1H, m), 3.51 (1H, dt), 3.66 (1H, dd), 3.80 (2H, d), 4.01 (1H, dd), 4.21 (1H, d), 4.56 (1H, s), 6.99 (1H, s), 7.22 (1H, dd), 7.54 - 7.61 (1H, m), 7.94 (1H, d), 8.33 (1H, d), 11.75 (1H, s). MS-ESI *m/z* 413 [MH^+]. Chiral HPLC: (HP1100 System 4, 5 μm Chiralcel OJ-H (250 mm x 4.6 mm) column eluting with *iso*-hexane/EtOH/MeOH/TEA (50/25/25/0.1) Rf, 15.685 >99%.

(*R*)-4-(2-Chloro-6-(methylthiomethyl)pyrimidin-4-yl)-3-methylmorpholine (71). Compound **70** (see Ref.[16]) (17.0 g, 48.1 mmol) was dissolved in DMF (150 mL), to this was

added sodium methanethiolate (3.4 g, 48.1 mmol) and the reaction was stirred for 1 hour at 25 °C. The reaction mixture was quenched with water (50 mL) and then extracted with Et_2O (3 x 50 mL). The combined organic layers were dried over $MgSO_4$, filtered and then evaporated. The residue was purified by flash chromatography on silica, eluting with a gradient of 50 to 100% EtOAc in *iso*-hexane. Pure fractions were evaporated to afford **71** (12.63 g, 96%). ^{1}H NMR (400 MHz, DMSO-d6): 1.20 (3H, d), 2.07 (3H, s), 3.11 - 3.26 (1H, m), 3.44 (1H, td), 3.53 (2H, s), 3.59 (1H, dd), 3.71 (1H, d), 3.92 (1H, dd), 3.98 (1H, br s), 4.33 (1H, s), 6.77 (1H, s). MS-ESI *m*/*z* 274 [MH$^+$].

(3*R*)-4-(2-Chloro-6-[(methylsulfinyl)methyl]-4-pyrimidinyl)-3-methylmorpholine (R/S-72). Sodium meta-periodate (2.87 g, 13.44 mmol) was added in one portion to **71** (3.68 g, 13.44 mmol) in water (10 mL), EtOAc (20 mL) and MeOH (10 mL). The resulting solution was stirred at 20 °C for 16 hours. The reaction mixture was diluted with DCM (60 mL) and then filtered. The DCM layer was separated and the aqueous layer washed with DCM (3 x 40 mL). The organic layers were combined, dried over $MgSO_4$, filtered and then evaporated. The residue was purified by flash chromatography on silica, eluting with a gradient of 0 to 7% MeOH in DCM. Pure fractions were evaporated to afford **R/S-72** (2.72 g, 70%). ^{1}H NMR (400 MHz, DMSO-d6): 1.22 (3H, d), 2.64 (3H, d), 3.14 - 3.26 (1H, m), 3.45 (1H, td), 3.59 (1H, dd), 3.73 (1H, d), 3.88 - 3.96 (2H, m), 4.00 (1H, d), 4.07 (1H, dt), 4.33 (1H, s), 6.81 (1H, s). MS-ESI *m*/*z* 290 [MH$^+$].

(*R*)-4-(2-Chloro-6-((*S*)-methylsulfinylmethyl)pyrimidin-4-yl)-3-methylmorpholine (S-72) and (*R*)-4-(2-chloro-6-((*R*)-methylsulfinylmethyl)pyrimidin-4-yl)-3-methylmorpholine (R-72). Compound **R/S-72** (2.7 g, 9.32 mmol) was purified by preparative chiral chromatography on a Merck 100 mm 20 μm Chiralpak AD column, eluting isocratically with a 50:50:0.1 mixture of *iso*-hexane:EtOH:TEA as eluent. The fractions containing product were evaporated to afford **S-72** (1.38 g, 51%) as the first eluting compound. ^{1}H NMR ($CDCl_3$): 1.29 (3H, dd), 2.56 (3H, s), 3.15 - 3.33 (1H, m), 3.46 (1H, tt), 3.55 - 3.83 (3H, m), 3.85 - 4.06 (3H, m), 4.31 (1H, s), 6.37 (1H, s). Chiral HPLC: (HP1100 System 6, 20μm Chiralpak AD (250 mm x 4.6 mm) column eluting with *iso*-hexane/EtOH/TEA 50/50/0.1) Rf, 7.197 > 99% and **R-72** (1.27 g, 47 %) as the second eluting compound. ^{1}H NMR (400 MHz, $CDCl_3$): 1.28 (3H, d), 2.58 (3H, s), 3.26 (1H, td), 3.48 (1H, td), 3.62 (1H, dt), 3.77 (2H, dd), 3.88 - 4.13 (3H, m), 4.28 (1H, s), 6.37 (1H, s). Chiral HPLC: (HP1100 System 6, 20μm Chiralpak AD (250 mm x 4.6 mm) column eluting with *iso*-hexane/EtOH/TEA 50/50/0.1) Rf, 16.897 > 99%.

Compound **R-72** was prepared on a large scale as follows:

Sodium meta-periodate (960 g, 4488.24 mmol) was added portionwise to **71** (1024 g, 3740.20 mmol) in water (3000 mL), EtOAc (6000 mL) and MeOH (3000 mL). The resulting solution was stirred at 17 °C for 16 hours. The reaction was diluted with DCM (18000 mL) and water (3000 mL). The DCM layer was separated and the water layer washed with DCM (3x 5000 mL). The organics were combined and dried over $MgSO_4$ and sodium bisulphite, filtered and evaporated. The crude product was purified by flash chromatography on silica, eluting with a

gradient of 10 to 50% MeOH in EtOAc. Pure fractions were evaporated to dryness to afford **R/S-72** (935 g, 86%).

Compound **R/S-72** (1933 g, 6670.58 mmol) was purified by preparative chiral chromatography on a Merck 100 mm 20 μm Chiralpak AD column, eluting isocratically with a 50:50:0.1 mixture of *iso*-hexane:EtOH:TEA as eluent. The fractions containing product were evaporated to afford **R-72** (886.4 g, 46%) as the second eluting compound. ^{1}H NMR (400 MHz, $CDCl_3$, 30 °C): 1.28 (3H, d), 2.58 (3H, s), 3.26 (1H, td), 3.48 (1H, td), 3.62 (1H, dt), 3.77 (2H, dd), 3.88 - 4.13 (3H, m), 4.28 (1H, s), 6.37 (1H, s). MS-ESI *m/z* 290, 292 [MH^+]. Chiral HPLC: (20μm Chiralpak AD (250 mm x 4.6 mm) column eluting with *iso*-hexane/EtOH/TEA 50/50/0.1) Rf, 16.897 > 99%.

N-[({2-Chloro-6-[(3*R*)-3-methylmorpholin-4-yl]pyrimidin-4-yl}methyl)(methyl)oxido-λ6-sulfanylidene]-2,2,2-trifluoroacetamide (R/S-74). Iodobenzene diacetate (6.54 g, 20.29 mmol) was added to **R/S-72** (5.88 g, 20.29 mmol), 2,2,2-trifluoroacetamide (4.59 g, 40.58 mmol), magnesium oxide (3.27 g, 81.16 mmol) and rhodium(II) acetate dimer (0.224 g, 0.51 mmol) in DCM (169 mL) under air. The resulting suspension was stirred at room temperature for 3 days. Further 2,2,2-trifluoroacetamide (1.15 g, 10.15 mmol), magnesium oxide (0.818 g, 20.29 mmol), rhodium(II) acetate dimer (0.056 g, 0.13 mmol) and iodobenzene diacetate (l .64 g, 5.07 mmol) were added and the suspension was stirred at room temperature for a further 24 hours. The reaction mixture was filtered and silica gel (3 g) was added to the filtrate and then the mixture was evaporated. The resulting powder was purified by flash chromatography on silica, eluting with a gradient of 20 to 50% EtOAc in *iso*-hexane. Fractions containing product were

evaporated and the residue was triturated with *iso*-hexane/MTBE to give a solid which was collected by filtration and dried under vacuum to afford **R/S-74** (6.64 g, 82%). ^{1}H NMR (400 MHz, $CDC1_3$): 1.33 (3H, d), 3.28 (1H, dd), 3.43 (3H, d), 3.46 - 3.59 (1H, m), 3.62 - 3.71 (1H, m), 3.79 (1H, d), 3.90 - 4.50 (2H, br s), 4.21 (1H, s), 4.66 (1H, dd), 4.86 (1H, dd), 6.50 (1H, d). MS-ESI *m/z* 401, 403 [MH^+].

***N*-[({2-Chloro-6-[(3*R*)-3-methylmorpholin-4-yl]pyrimidin-4-yl}methyl)(*R*-methyl)oxido-λ6-sulfanylidene]-2,2,2-trifluoroacetamide (R-74)**. To a stirring solution of **R-72** (285 g, 983.50 mmol) in DCM (2810 mL) was added magnesium oxide (159 g, 3934.00 mmol), iodobenzene diacetate (475 g, 1475.25 mmol), rhodium(II) acetate dimer (10.87 g, 24.59 mmol) and 2,2,2-trifluoroacetamide (222 g, 1967.00 mmol). The mixture was maintained at room temperature under air for 16 hours. The resultant light brown suspension was removed by filtration. The filtrate was evaporated then purified by flash chromatography on silica, eluting with a gradient of 30 to 100% EtOAc in heptane. Pure fractions were evaporated to afford **R-74** (306 g, 77%). ^{1}H NMR (400 MHz, $CDCl_3$, 30 °C): 1.33 (3H, d), 3.25 - 3.38 (1H, m), 3.42 (3H, s), 3.51 (1H, td), 3.66 (1H, dd), 3.79 (1H, d), 4.01 (1H, dd), 4.31 (1H, s), 4.64 (1H, d), 4.77 - 4.87 (1H, m), 6.48 (1H, d). MS-ESI *m/z* 401, 403 [MH^+].

(3*R*)-4-(2-Chloro-6-(1-(S-methylsulfonimidoyl)cyclopropyl)pyrimidin-4-yl)-3-methylmorpholine (R/S-75). Sodium hydroxide (50% aq.) (217 mL, 4059.84 mmol) was added to **R/S-74** (27.12 g, 67.66 mmol), 1,2-dibromoethane (23.3 mL, 270.66 mmol) and

tetraoctylammonium bromide (3.70 g, 6.77 mmol) in methyl THF (1000 mL) at 20 °C under nitrogen. The resulting mixture was stirred at 20 °C for 24 hours. Further 1,2-dibromoethane (23.3 mL, 270.66 mmol) was added and the mixture was stirred at 20 °C for a further 24 hours. The reaction mixture was diluted with mTHF (1000 mL) and the aqueous layer separated. The organic layer was diluted further with EtOAc (1000 mL) and washed with water (1500 mL). The organic layer was dried over $MgSO_4$, filtered and then evaporated. The residue was purified by flash chromatography on silica, eluting with a gradient of 0 to 5% MeOH in DCM. Pure fractions were evaporated to afford **R/S-75** (14.80 g, 66%). ^{1}H NMR (400 MHz, DMSO-d6): 1.21 (3H, d), 1.39 (3H, m), 1.62 - 1.71 (1H, m), 3.01 (3H, s), 3.43 (1H, tt), 3.58 (1H, dd), 3.72 (1H, d), 3.82 (1H, d), 3.93 (1H, dd), 4.01 (1H, s), 4.38 (1H, s), 6.96 (1H, d). MS-ESI *m/z* 331, 333 [MH^+].

(3*R*)-4-(2-Chloro-6-(1-((*R*)-*S*-methylsulfonimidoyl)cyclopropyl)pyrimidin-4-yl)-3-methylmorpholine (R-75). To a solution of **R-74** (476 g, 1188 mmol), 1,2-dibromoethane (1023 mL, 11876 mmol) and tetra-octylammonium bromide (64.9 g, 118.76 mmol) in mTHF (4750 mL) was added sodium hydroxide (3170 mL, 59380.59 mmol) over 10 min. The mixture was stirred for 4 hours at room temperature. The organic layer was separated, washed with brine (2000 mL) and dried over $MgSO_4$ then filtered. The filtrate was evaporated then purified by flash chromatography on silica, eluting with a gradient of 0 to 5% MeOH in EtOAc. Pure fractions were evaporated to afford **R-75** (259 g, 66%). ^{1}H NMR (400 MHz, DMSO-d6): 1.14 - 1.21 (m, 4 H) 1.22 - 1.32 (m, 7 H) 1.34 - 1.47 (m, 3 H) 1.56 (br. s., 1 H) 1.59 - 1.71 (m, 1 H) 3.00

(d, *J*=1.27 Hz, 3 H) 3.09 - 3.23 (m, 2 H) 3.29 (s, 2 H) 3.42 (td, *J*=11.85, 2.91 Hz, 1 H) 3.57 (dd, *J*=11.53, 3.17 Hz, 1 H) 3.70 (d, *J*=11.41 Hz, 1 H) 3.81 (s, 1 H) 3.92 (dd, *J*=11.53, 3.68 Hz, 1 H) 3.95 - 4.13 (m, 1 H) 4.37 (br s, 1 H) 6.95 (s, 1 H). MS-ESI *m/z* 331, 333 [MH^+].

Biological Evaluation. IC_{50} values reported are geometric mean values of at least two independent measurements unless otherwise stated.

Cell line studies. Cells lines were grown in RPMI-1640 media, 10% FCS, 2 mmol/L glutamine at 37 °C/5% CO_2 unless indicated otherwise. All cell lines were authenticated via the AstraZeneca (AZ) Cell Bank using DNA fingerprinting short tandem repeat (STR) assays. All revived cells were used within 20 passages, and cultured for less than 6 months.

ATR Kinase Assay. As described in Foote *et al.* [16]

ATR Cell (pChk1) Assay in HT29 Tumor Cells. Assay is a variation on that described in Foote *et al.*,[16] with the use of alterative primary pCHK1 S345 antibodies (Cell Signaling Technologies) and secondary AlexaFluor-488 antibody (Molecular Probes).

***In Vivo* Studies.** All animal experiments were conducted in full accordance with the U.K. Home Office Animal (Scientific Procedures) Act 1986. Anti-tumor studies: Female Swiss nu/nu mice (AstraZeneca, U.K.) were housed in negative pressure isolators (PFI Systems Ltd., Oxon, U.K.). LoVo tumor xenografts were established in 8- to 12-week-old mice by injecting 1×10^7 tumor cells subcutaneously (100 μL in serum free medium) on the left dorsal flank. Animals were randomized into treatment groups when tumors became palpable. Compound **2** was administered orally. Tumors were measured up to three times per week with calipers. Tumor

volumes were calculated and the data plotted using the geometric mean for each group versus time.

γH2AX Immunohistochemistry pharmacodynamic analysis (PD): 4 tumors were used per point. Sections of tissue 4 μm were cut on a microtome (Thermo Fisher Scientific) and mounted on electrostatically charged glass slides (Thermo Fisher Scientific). Sections were de-waxed in xylene, passed through graded alcohols and rehydrated in water. Heat mediated antigen retrieval was performed using a RHS2 microwave (Milestone) at 110 °C for two min in pH 9.0 Target Retrieval Solution (cat. #S2367, Dako UK Ltd). Immunohistochemistry was then performed at room temperature on a Lab Vision Autostainer 480 (Lab Vision). 0.05 M Tris buffered saline with 0.1% Tween 20 (TBST), pH 7.6 was used for both the reagent and wash buffers. Sections were treated with 10% hydrogen peroxide in TBST for 10 min, washed and incubated with Background Blocker (cat. #MP-966-P500, A.Menarini Diagnostics Ltd) for 20 min. Sections were incubated with anti-phospho-Ser139 (γ)H2AX (cat. #2577, Cell Signalling Technology) for 1 hours before washing and incubating with X-Cell Polymer HRP for fifteen min before being visualised by incubation with the chromogen, diaminbenzidine (DAB) (cat. #MP-, A.Menarini Diagnostics Ltd), for 10 min. Sections were washed for 10 min in H_2O and counterstained with Carrazzis haematoxylin (Clin-Tech), dehydrated though graded IMS, cleared in xylene and mounted using glass coverslips and Histomount (RA Lamb). Slides were scanned and digitized using an Scanscope XT slide scanner (Aperio) at x20 magnification. Once scanned, all digital images representing whole tissue sections, were evaluated for image quality. Immunohistochemistry staining was then quantified using the Spectrum Analysis

algorithm package and Image Scope viewing software (Aperio). Data are presented as % γH2AX positive tissue from total tissue area counted, through quantification of pixel counts for γH2AX positive c (brown) and Hematoxylin only tissue (blue) staining. Only viable tumor was included in the analysis (necrotic area were excluded). Four independent mouse tumors were analysed per time point.

ANCILLARY INFORMATION

Supporting information

Figure S1: Kinome tree graphs for **3**, **21**, **15**. Table S1: kinase inhibition data for **2**. Table S2: ATR activity data for **37**, **38**. Scheme S1: synthetic route to **37**, **38**. Crystallisation methods for compound **2**. Experimental details and data for compounds **5** – **32**, **34** - **38**, **40** – **45**, **50** - **69**, **R/S-73**, **77** – **79**. Crystal formation method of **R-72**. Figure S2: X-ray structure of **R-72**. Aqueous solubility, $LogD_{7.4}$ methods.

Molecular formula strings are available in a separate file.

Corresponding Author

* Dr. J. Willem M. Nissink, email: willem.nissink@astrazeneca.com

Author Contributions

The manuscript was written through contributions of all authors. All authors were employees of AstraZeneca at the time of the described work, and have given approval to the final version of the manuscript.

Acknowledgments

We acknowledge Lorraine Hassall, Craig Robertson, Jessica Boyd and Adrian Pickup for their contribution to chemical synthesis; Darren Cumberbatch, Graeme Scarfe, and Kin Tam for DMPK and physicochemical property characterization; Adina Hughes and Elaine Brown for biological experiments and cell assays; Anne Ertan for small-molecule crystal structure processing; Jennifer Barnes for help with *in vivo* experiments Kristin Goldberg for help with preparing the manuscript; and past and present members of the ATR project.

Abbreviations. The following abbreviations are used: ACN, acetonitrile; API, active pharmaceutical ingredient; ATM, Ataxia telangiectasia mutated; ATR, Ataxia telangiectasia mutated and rad3 related; AUC, area under the curve; BD, *bis in die* – twice daily; CLint, intrinsic clearance; CYP3A4, cyptochrome P450 3A4 isoform; D_{abs}, maximum absorbable dose; DCM, dichloromethane; DDI, drug-drug interaction; DDR, DNA-damage response; DIPEA, di*iso*propylethylamine; DMA, *N*,*N*-dimethylacetamide; DMAP, 4-dimethylaminopyridine; DME, 1,2-dimethoxyethane; DMF, *N*,*N*-dimethylformamide; DMSO, dimethylsulfoxide; DNA-PK, DNA-dependent protein kinase; DSB, double strand breaks; Et_2O, diethylether;

EtOAc, ethyl acetate; EtOH, ethanol; γ-H2AX, variant histone H2A, phosphorylated; GSH, glutathione; hERG, human ether-a-go-go-related gene; IND, Investigational New Drug; IPA, 2-propanol; LCMS, liquid chromatography mass spectrometer; IR, ionizing radiation; MeOH, methanol; mTHF, 2-methyltetrahydrofuran; MTBE, methyl *tert*-butylether; mTOR, mammalian target of Rapamycin; PBPK, physiologically based pharmacokinetics; PK, pharmacokinetics; PIKK, phosphatidylinositol 3-kinase-related kinase; PI3K, phosphatidylinositol 3-kinase; RSR, replication stress response; SAR, structure activity relationship; SOC, standard of care; TDI, time-dependent inhibitor; TFA, trifluoroacetic acid; THF, tetrahydrofuran; TGI, tumor growth inhibition; Vd_{ss}, volume of distribution at steady state; QD, *quaque die* – once daily.

REFERENCES

1. O'Connor, M. J. Targeting the DNA damage response in cancer. *Mol. Cell.* **2015,** 60, 547-560.

2. Jackson, S. P.; Helleday, T. DNA Repair. Drugging DNA repair. *Science* **2016,** 352, 1178-1179.

3. Yazinski, S. A.; Zou, L. Functions, regulation, and therapeutic implications of the ATR checkpoint pathway. *Annu. Rev. Genet.* **2016,** 50, 155-173.

4. Cimprich, K. A.; Cortez, D. ATR: an essential regulator of genome integrity. *Nat. Rev. Mol. Cell. Biol.* **2008,** 9, 616-627.

5. Macheret, M.; Halazonetis, T. D. DNA replication stress as a hallmark of cancer. *Annu. Rev. Pathol.* **2015,** 10, 425-448.

6. Foote, K. M.; Lau, A.; Nissink, J. W. Drugging ATR: progress in the development of specific inhibitors for the treatment of cancer. *Future Med. Chem.* **2015,** 7, 873-891.

7. Weber, A. M.; Ryan, A. J. ATM and ATR as therapeutic targets in cancer. *Pharmacol. Ther.* **2015,** 149, 124-138.

8. Sundar, R.; Brown, J.; Ingles Russo, A.; Yap, T. A. Targeting ATR in cancer medicine. *Curr. Probl. Cancer* **2017,** 41, 302-315.

9. Rundle, S.; Bradbury, A.; Drew, Y.; Curtin, N. J. Targeting the ATR-CHK1 axis in cancer therapy. *Cancers (Basel)* **2017,** 9, E41.

10. Kwok, M.; Davies, N.; Agathanggelou, A.; Smith, E.; Oldreive, C.; Petermann, E.; Stewart, G.; Brown, J.; Lau, A.; Pratt, G.; Parry, H.; Taylor, M.; Moss, P.; Hillmen, P.; Stankovic, T. ATR inhibition induces synthetic lethality and overcomes chemoresistance in TP53- or ATM-defective chronic lymphocytic leukemia cells. *Blood* **2016,** 127, 582-595.

11. Min, A.; Im, S. A.; Jang, H.; Kim, S.; Lee, M.; Kim, D. K.; Yang, Y.; Kim, H. J.; Lee, K. H.; Kim, J. W.; Kim, T. Y.; Oh, D. Y.; Brown, J.; Lau, A.; O'Connor, M. J.; Bang, Y. J. AZD6738, a novel oral inhibitor of ATR, induces synthetic lethality with ATM deficiency in gastric cancer cells. *Mol. Cancer. Ther.* **2017,** 16, 566-577.

12. Vendetti, F. P.; Lau, A.; Schamus, S.; Conrads, T. P.; O'Connor, M. J.; Bakkenist, C. J. The orally active and bioavailable ATR kinase inhibitor AZD6738 potentiates the anti-tumor effects of cisplatin to resolve ATM-deficient non-small cell lung cancer in vivo. *Oncotarget* **2015,** 6, 44289-44305.

13. Dillon, M. T.; Barker, H. E.; Pedersen, M.; Hafsi, H.; Bhide, S. A.; Newbold, K. L.; Nutting, C. M.; McLaughlin, M.; Harrington, K. J. Radiosensitization by the ATR inhibitor AZD6738 through generation of acentric micronuclei. *Mol. Cancer. Ther.* **2017,** 16, 25-34.

14. Dunne, V.; Ghita, M.; Small, D. M.; Coffey, C. B. M.; Weldon, S.; Taggart, C. C.; Osman, S. O.; McGarry, C. K.; Prise, K. M.; Hanna, G. G.; Butterworth, K. T. Inhibition of ataxia telangiectasia related-3 (ATR) improves therapeutic index in preclinical models of non-small cell lung cancer (NSCLC) radiotherapy. *Radiother. Oncol.* **2017,** 124, 475-481.

15. Kim, H.; George, E.; Ragland, R.; Rafial, S.; Zhang, R.; Krepler, C.; Morgan, M.; Herlyn, M.; Brown, E.; Simpkins, F. Targeting the ATR/CHK1 axis with PARP inhibition results in tumor regression in BRCA-mutant ovarian cancer models. *Clin. Cancer Res.* **2017,** 23, 3097-3108.

16. Foote, K. M.; Blades, K.; Cronin, A.; Fillery, S.; Guichard, S. S.; Hassall, L.; Hickson, I.; Jacq, X.; Jewsbury, P. J.; McGuire, T. M.; Nissink, J. W.; Odedra, R.; Page, K.; Perkins, P.; Suleman, A.; Tam, K.; Thommes, P.; Broadhurst, R.; Wood, C. Discovery of 4-{4-[(3R)-3-Methylmorpholin-4-yl]-6-[1-(methylsulfonyl)cyclopropyl]pyrimidin-2-y l}-1H-indole

(AZ20): a potent and selective inhibitor of ATR protein kinase with monotherapy in vivo antitumor activity. *J. Med. Chem.* **2013,** 56, 2125-2138.

17. Menezes, D. L.; Holt, J.; Tang, Y.; Feng, J.; Barsanti, P.; Pan, Y.; Ghoddusi, M.; Zhang, W.; Thomas, G.; Holash, J.; Lees, E.; Taricani, L. A synthetic lethal screen reveals enhanced sensitivity to ATR inhibitor treatment in mantle cell lymphoma with ATM loss-of-function. *Mol. Cancer Res.* **2015,** 13, 120-129.

18. Wengner, A. S., G; Luecking, U; Lefranc, J; Lienau, P; Deeg, G; Lagkadinou, E; Liu, L; Golfier, S; Schatz, C; Scholz, A; von Nussbaum, F; Brands, M; Mumberg, D; Ziegelbauer, K. In *ATR Inhibitor BAY 1895344 Shows Potent Anti-tumor Efficacy in Monotherapy and Strong Combination Potential with the Targeted Alpha Therapy Radium-223 Dichloride in Preclinical Tumor Models*, AACR, Washington, DC. Philadelphia (PA), 2017.

19. Ishiyama, T.; Murata, M.; Miyaura, N. Palladium(0)-catalyzed cross-coupling reaction of alkoxydiboron with haloarenes: a direct procedure for arylboronic esters. *J. Org. Chem.* **1995,** 60, 7508-7510.

20. Goundry, W. R. F.; Adams, B.; Benson, H.; Demeritt, J.; McKown, S.; Mulholland, K.; Robertson, A.; Siedlecki, P.; Tomlin, P.; Vare, K. Development and scale-up of a biocatalytic process to form a chiral sulfoxide. *Org. Process Res. Dev.* **2017,** 21, 107-113.

21. Okamura, H.; Bolm, C. Rhodium-catalyzed imination of sulfoxides and sulfides: efficient preparation of N-unsubstituted sulfoximines and sulfilimines. *Org. Lett.* **2004,** 6, 1305-1307.

22. Dresser, G. K.; Spence, J. D.; Bailey, D. G. Pharmacokinetic-pharmacodynamic consequences and clinical relevance of cytochrome P450 3A4 inhibition. *Clin. Pharmacokinet.* **2000,** 38, 41-57.

23. Kalgutkar, A. S.; Obach, R. S.; Maurer, T. S. Mechanism-based inactivation of cytochrome P450 enzymes: chemical mechanisms, structure-activity relationships and relationship to clinical drug-drug interactions and idiosyncratic adverse drug reactions. *Curr. Drug. Metab.* **2007,** 8, 407-447.

24. Hollenberg, P. F.; Kent, U. M.; Bumpus, N. N. Mechanism-based inactivation of human cytochromes p450s: experimental characterization, reactive intermediates, and clinical implications. *Chem. Res. Toxicol.* **2008,** 21, 189-205.

25. Curatolo, W. Physical chemical properties of oral drug candidates in the discovery and exploratory development settings. *Pharm. Sci. & Tech. Today* **1998,** 1, 387-393.

26. Kenny, J. R.; Mukadam, S.; Zhang, C.; Tay, S.; Collins, C.; Galetin, A.; Khojasteh, S. C. Drug-drug interaction potential of marketed oncology drugs: in vitro assessment of time-dependent cytochrome P450 inhibition, reactive metabolite formation and drug-drug interaction prediction. *Pharm. Res.* **2012,** 29, 1960-1976.

27. Stepan, A. F.; Walker, D. P.; Bauman, J.; Price, D. A.; Baillie, T. A.; Kalgutkar, A. S.; Aleo, M. D. Structural alert/reactive metabolite concept as applied in medicinal chemistry to mitigate the risk of idiosyncratic drug toxicity: a perspective based on the critical examination of trends in the top 200 drugs marketed in the United States. *Chem. Res. Toxicol.* **2011,** 24, 1345-1410.

28. Cytochrome P450 3A4 and 3A5 Known Drug Interaction Chart. *URL: http://www.mayomedicallaboratories.com/it-mmfiles/Cytochrome_P450_3A4_and_3A5_Known_Drug_Interaction_Chart.pdf* (accessed June 5, 2018).

29. Overton, M.; Hickman, J. A.; Threadgill, M. D.; Vaughan, K.; Gescher, A. The generation of potentially toxic, reactive iminium ions from the oxidative metabolism of xenobiotic N-alkyl compounds. *Biochem. Pharmacol.* **1985,** 34, 2055-2061.

30. Masic, L. P. Role of cyclic tertiary amine bioactivation to reactive iminium species: structure toxicity relationship. *Curr. Drug Metab.* **2011,** 12, 35-50.

31. Bolleddula, J.; DeMent, K.; Driscoll, J. P.; Worboys, P.; Brassil, P. J.; Bourdet, D. L. Biotransformation and bioactivation reactions of alicyclic amines in drug molecules. *Drug. Metab. Rev.* **2014,** 46, 379-419.

32. Dalvie, D. K.; Kalgutkar, A. S.; Khojasteh-Bakht, S. C.; Obach, R. S.; O'Donnell, J. P. Biotransformation reactions of five-membered aromatic heterocyclic rings. *Chem. Res. Toxicol.* **2002,** 15, 269-299.

33. Inoue, K.; Fukuda, K.; Yoshimura, T.; Kusano, K. Comparison of the reactivity of trapping reagents toward electrophiles: cysteine derivatives can be bifunctional trapping reagents. *Chem. Res. Toxicol.* **2015,** 28, 1546-1555.

34. Atkinson, A.; Kenny, J. R.; Grime, K. Automated assessment of time-dependent inhibition of human cytochrome P450 enzymes using liquid chromatography-tandem mass spectrometry analysis. *Drug. Metab. Dispos.* **2005,** 33, 1637-1647.

35. Kaplan, J.; Verheijen, J. C.; Brooijmans, N.; Toral-Barza, L.; Hollander, I.; Yu, K.; Zask, A. Discovery of 3,6-dihydro-2H-pyran as a morpholine replacement in 6-aryl-1H-pyrazolo[3,4-d]pyrimidines and 2-arylthieno[3,2-d]pyrimidines: ATP-competitive inhibitors of the mammalian target of rapamycin (mTOR). *Bioorg. Med. Chem. Lett.* **2010,** 20, 640-643.

36. Zask, A.; Kaplan, J.; Verheijen, J. C.; Richard, D. J.; Curran, K.; Brooijmans, N.; Bennett, E. M.; Toral-Barza, L.; Hollander, I.; Ayral-Kaloustian, S.; Yu, K. Morpholine derivatives greatly enhance the selectivity of mammalian target of rapamycin (mTOR) inhibitors. *J. Med. Chem.* **2009,** 52, 7942-7945.

37. Safina, B. S.; Baker, S.; Baumgardner, M.; Blaney, P. M.; Chan, B. K.; Chen, Y. H.; Cartwright, M. W.; Castanedo, G.; Chabot, C.; Cheguillaume, A. J.; Goldsmith, P.; Goldstein,

D. M.; Goyal, B.; Hancox, T.; Handa, R. K.; Iyer, P. S.; Kaur, J.; Kondru, R.; Kenny, J. R.; Krintel, S. L.; Li, J.; Lesnick, J.; Lucas, M. C.; Lewis, C.; Mukadam, S.; Murray, J.; Nadin, A. J.; Nonomiya, J.; Padilla, F.; Palmer, W. S.; Pang, J.; Pegg, N.; Price, S.; Reif, K.; Salphati, L.; Savy, P. A.; Seward, E. M.; Shuttleworth, S.; Sohal, S.; Sweeney, Z. K.; Tay, S.; Tivitmahaisoon, P.; Waszkowycz, B.; Wei, B.; Yue, Q.; Zhang, C.; Sutherlin, D. P. Discovery of novel PI3-kinase delta specific inhibitors for the treatment of rheumatoid arthritis: taming CYP3A4 time-dependent inhibition. *J. Med. Chem.* **2012,** 55, 5887-5900.

38. Pennington, L. D.; Moustakas, D. T. The necessary nitrogen atom: a versatile high-impact design element for multiparameter optimization. *J. Med. Chem.* **2017,** 60, 3552-3579.

39. Lu, Y.; Knapp, M.; Crawford, K.; Warne, R.; Elling, R.; Yan, K.; Doyle, M.; Pardee, G.; Zhang, L.; Ma, S.; Mamo, M.; Ornelas, E.; Pan, Y.; Bussiere, D.; Jansen, J.; Zaror, I.; Lai, A.; Barsanti, P.; Sim, J. Rationally designed PI3Kalpha mutants to mimic ATR and their use to understand binding specificity of ATR inhibitors. *J. Mol. Biol.* **2017,** 429, 1684-1704.

40. Rao, Q.; Liu, M.; Tian, Y.; Wu, Z.; Hao, Y.; Song, L.; Qin, Z.; Ding, C.; Wang, H. W.; Wang, J.; Xu, Y. Cryo-EM structure of human ATR-ATRIP complex. *Cell Res.* **2018,** 28, 143-156.

41. Terrine, K. A., A. Diazaindenes ('azaindoles') - Part I. Ionisation constants and spectra. *J. Chem. Soc.* **1960,** 0, 1794-1797.

42. Kawashima, S. M., T.; Yaguchi, S.; Sasahara, H.; Watanabe, T. , Heterocyclic Compound and Antitumor Agent Containing the Same as Active Ingredient, WO2002088112, 2002.

43. Scott, J. S.; Birch, A. M.; Brocklehurst, K. J.; Broo, A.; Brown, H. S.; Butlin, R. J.; Clarke, D. S.; Davidsson, O.; Ertan, A.; Goldberg, K.; Groombridge, S. D.; Hudson, J. A.; Laber, D.; Leach, A. G.; Macfaul, P. A.; McKerrecher, D.; Pickup, A.; Schofield, P.; Svensson, P. H.; Sorme, P.; Teague, J. Use of small-molecule crystal structures to address solubility in a novel series of G protein coupled receptor 119 agonists: optimization of a lead and in vivo evaluation. *J. Med. Chem.* **2012,** 55, 5361-5379.

44. Lucking, U. Sulfoximines: a neglected opportunity in medicinal chemistry. *Angew. Chem. Int. Ed. Engl.* **2013,** 52, 9399-9408.

45. Sirvent, J. A.; Lucking, U. Novel pieces for the emerging picture of sulfoximines in drug discovery: synthesis and evaluation of sulfoximine analogues of marketed drugs and advanced clinical candidates. *Chem. Med. Chem.* **2017,** 12, 487-501.

46. Frings, M.; Bolm, C.; Blum, A.; Gnamm, C. Sulfoximines from a Medicinal Chemist's Perspective: Physicochemical and in vitro Parameters Relevant for Drug Discovery. *Eur. J. Med. Chem.* **2017,** 126, 225-245.

47. Redfern, W. S.; Carlsson, L.; Davis, A. S.; Lynch, W. G.; MacKenzie, I.; Palethorpe, S.; Siegl, P. K.; Strang, I.; Sullivan, A. T.; Wallis, R.; Camm, A. J.; Hammond, T. G. Relationships between preclinical cardiac electrophysiology, clinical QT interval prolongation and torsade

de pointes for a broad range of drugs: evidence for a provisional safety margin in drug development. *Cardiovasc. Res.* **2003,** 58, 32-45.

48. Fokas, E.; Prevo, R.; Pollard, J. R.; Reaper, P. M.; Charlton, P. A.; Cornelissen, B.; Vallis, K. A.; Hammond, E. M.; Olcina, M. M.; Gillies McKenna, W.; Muschel, R. J.; Brunner, T. B. Targeting ATR in vivo using the novel inhibitor VE-822 results in selective sensitization of pancreatic tumors to radiation. *Cell Death Dis.* **2012,** 3, e441.

49. Jacq, X. S., L.; Brown, E. AZ20, Aa novel potent and selective inhibitor of ATR kinase with invivo antitumour activity. In *Cancer Res.* , 2012; Vol. 72(8 Suppl. 1) Abstract 1823.

50. Barlaam, B.; Cosulich, S.; Degorce, S.; Fitzek, M.; Green, S.; Hancox, U.; Lambert-van der Brempt, C.; Lohmann, J. J.; Maudet, M.; Morgentin, R.; Pasquet, M. J.; Peru, A.; Ple, P.; Saleh, T.; Vautier, M.; Walker, M.; Ward, L.; Warin, N. Discovery of (R)-8-(1-(3,5-difluorophenylamino)ethyl)-N,N-dimethyl-2-morpholino-4-oxo-4H-chrom ene-6-carboxamide (AZD8186): a potent and selective inhibitor of PI3Kbeta and PI3Kdelta for the treatment of PTEN-deficient cancers. *J. Med. Chem.* **2015,** 58, 943-962.

51. Barlaam, B.; Cosulich, S.; Delouvrie, B.; Ellston, R.; Fitzek, M.; Germain, H.; Green, S.; Hancox, U.; Harris, C. S.; Hudson, K.; Lambert-van der Brempt, C.; Lebraud, H.; Magnien, F.; Lamorlette, M.; Le Griffon, A.; Morgentin, R.; Ouvry, G.; Page, K.; Pasquet, G.; Polanska, U.; Ruston, L.; Saleh, T.; Vautier, M.; Ward, L. Discovery of 1-(4-(5-(5-amino-6-(5-tert-butyl-1,3,4-oxadiazol-2-yl)pyrazin-2-yl)-1-ethyl-1,2,4 -triazol-3-yl)piperidin-1-yl)-3-

hydroxypropan-1-one (AZD8835): A potent and selective inhibitor of PI3Kalpha and PI3Kdelta for the treatment of cancers. *Bioorg. Med. Chem. Lett.* **2015,** 25, 5155-5162.

52. Bonner, W. M.; Redon, C. E.; Dickey, J. S.; Nakamura, A. J.; Sedelnikova, O. A.; Solier, S.; Pommier, Y. GammaH2AX and cancer. *Nat. Rev. Cancer* **2008,** 8, 957-967.

53. Chen, T.; Middleton, F. K.; Falcon, S.; Reaper, P. M.; Pollard, J. R.; Curtin, N. J. Development of pharmacodynamic biomarkers for ATR inhibitors. *Mol. Oncol.* **2015,** 9, 463-472.

54. Nestorov, I. A.; Aarons, L. J.; Arundel, P. A.; Rowland, M. Lumping of whole-body physiologically based pharmacokinetic models. *J. Pharmacokinet. Biopharm.* **1998,** 26, 21-46.

55. Luttringer, O.; Theil, F. P.; Poulin, P.; Schmitt-Hoffmann, A. H.; Guentert, T. W.; Lave, T. Physiologically based pharmacokinetic (PBPK) modeling of disposition of epiroprim in humans. *J. Pharm. Sci.* **2003,** 92, 1990-2007.

56. Sjogren, E.; Westergren, J.; Grant, I.; Hanisch, G.; Lindfors, L.; Lennernas, H.; Abrahamsson, B.; Tannergren, C. In silico predictions of gastrointestinal drug absorption in pharmaceutical product development: application of the mechanistic absorption model GI-Sim. *Eur. J. Pharm. Sci.* **2013,** 49, 679-698.

57. Ding, X.; Rose, J. P.; Van Gelder, J. Developability assessment of clinical drug products with maximum absorbable doses. *Int. J. Pharm.* **2012,** 427, 260-269.

58. McGinnity, D. F.; Collington, J.; Austin, R. P.; Riley, R. J. Evaluation of human pharmacokinetics, therapeutic dose and exposure predictions using marketed oral drugs. *Curr. Drug Metab.* **2007,** 8, 463-479.

59. Sohlenius-Sternbeck, A. K.; Jones, C.; Ferguson, D.; Middleton, B. J.; Projean, D.; Floby, E.; Bylund, J.; Afzelius, L. Practical use of the regression offset approach for the prediction of in vivo intrinsic clearance from hepatocytes. *Xenobiotica* **2012,** 42, 841-853.

60. Yap, T. A.; Krebs, M. G.; Postel-Vinay, S.; Bang, Y. J.; El-Khoueiry, A.; Abida, W.; Harrington, K.; Sundar, R.; L. Carter, L.; Castanon-Alvarez, E.; S.A. Im, S. A.; Berges, A.; Khan, M.; Stephens, C.; Ross, G.; Soria, J. C. Phase I modular study of AZD6738, a novel oral, potent and selective ataxia telangiectasia Rad3-related (ATR) inhibitor in combination (combo) with carboplatin, olaparib or durvalumab in patients (pts) with advanced cancers *Eur. J. Cancer* **2016,** 69, S2.

61. Krebs, M. G.; Lopez, J.; El-Khoueiry, A.; Bang, Y.-J.; Postel-Vinay, S.; Abida, W.; Carter, L.; Xu, W.; Im, S.-A.; Pierce, A.; Frewer, P.; Berges, A.; Cheung, S. Y. A.; Stephens, C.; Felicetti, B.; Dean, E.; Hollingsworth, S. J. Phase I study of AZD6738, an inhibitor of ataxia telangiectasia Rad3-related (ATR), in combination with olaparib or durvalumab in patients (pts) with advanced solid cancers. In: Proceedings of the American Association for Cancer Research Annual Meeting **2018**; 2018 Apr 14-18; Chicago, IL. Philadelphia (PA): AACR; Cancer Res 2018;78(13 Suppl):Abstract nr CT026.

62. Berges, A.; Cheung, S. Y. A.; Pierce, A.; Dean, E.; Felicetti, B.; Standifer, N.; Smith, S.; Yates, J.; Lau, A.; Stephens, C.; Krebs, M. G.; K., H.; Hollingsworth, S. J. PK-Biomarker-Safety modelling aids choice of recommended Phase II dose and schedule for AZD6738 (ATR inhibitor). . In: Proceedings of the American Association for Cancer Research Annual Meeting **2018**; 2018 Apr 14-18; Chicago, IL. Philadelphia (PA): AACR; Cancer Res 2018;78(13 Suppl):Abstract nr CT118.

63. Lloyd, R.; Falenta, K.; Wijnhoven, P. W.; Chabbert, C.; Stott, J.; Yates, J.; Lau, A. Y.; Young, L. A.; Hollingsworth, S. J. The PARP inhibitor olaparib is synergistic with the ATR inhibitor AZD6738 in ATM deficient cancer cells. In: Proceedings of the American Association for Cancer Research Annual Meeting **2018**; 2018 Apr 14-18; Chicago, IL. Philadelphia (PA): AACR; Cancer Res 2018;78(13 Suppl):Abstract nr 337.

TABLE OF CONTENTS GRAPHIC

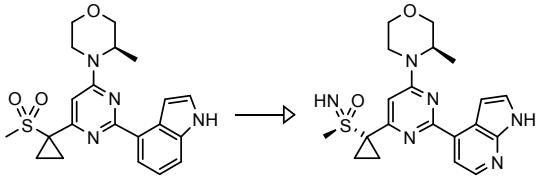

1; AZ20
ATR cell IC_{50} = 0.060μM
Low aqueous solubility
CYP3A4 TDI

In vivo tool compound

2; AZD6738
ATR cell IC_{50} = 0.074μM
High aqueous solubility
No CYP3A4 TDI

Clinical candidate